Cell Stem Cell

Short article

Epitranscriptomic regulation of cortical neurogenesis via Mettl8-dependent mitochondrial tRNA m^3C modification

Graphical abstract

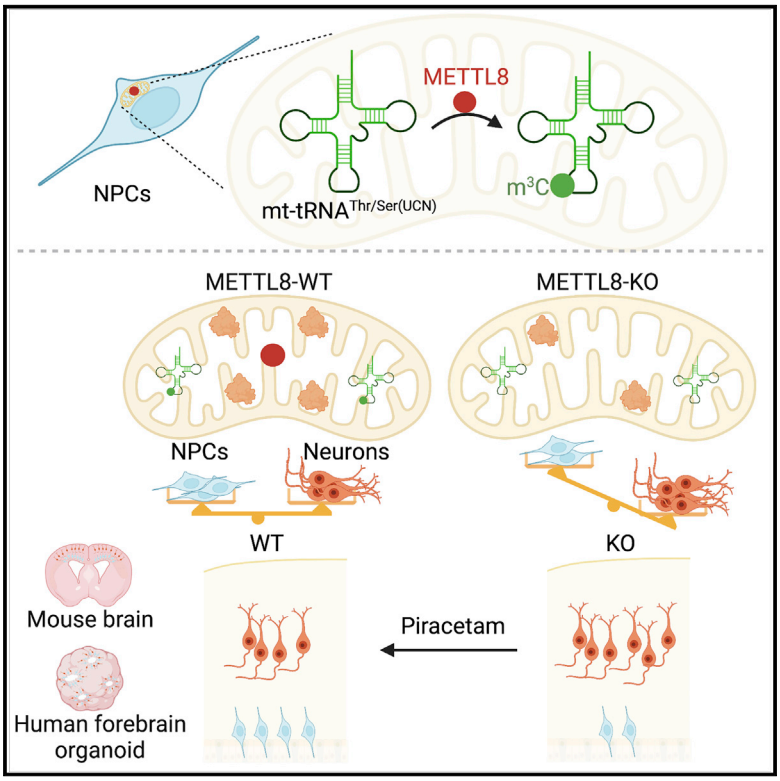

Highlights

- Mettl8 installs m^3C modification on mt-tRNA$^{Thr/Ser(UCN)}$ in cortical neural stem cells
- Mettl8 regulates mitochondrial protein translation and function in neural stem cells
- *Mettl8*-deleted mice exhibit accelerated embryonic cortical neural stem cell depletion
- METTL8 plays a conserved role in neurogenesis in human forebrain organoids as in mice

Authors

Feng Zhang, Kijun Yoon, Daniel Y. Zhang, Nam-Shik Kim, Guo-li Ming, Hongjun Song

Correspondence

gming@pennmedicine.upenn.edu (G.-l.M.), shongjun@pennmedicine.upenn.edu (H.S.)

In brief

Zhang et al. identified an epitranscriptomic mechanism regulating cortical neural stem cells in the embryonic mouse brain and human forebrain organoids. Specifically, Mettl8 installs m^3C modification on mitochondrial tRNA$^{Thr/Ser(UNC)}$, which regulates mitochondrial protein translation and function, and loss of Mettl8 leads to accelerated embryonic cortical neural stem cell depletion.

Zhang et al., 2023, Cell Stem Cell *30*, 1–12
March 2, 2023
https://doi.org/10.1016/j.stem.2023.01.007

CellPress

Please cite this article in press as: Zhang et al., Epitranscriptomic regulation of cortical neurogenesis via Mettl8-dependent mitochondrial tRNA m^3C modification, Cell Stem Cell (2023), https://doi.org/10.1016/j.stem.2023.01.007

Cell Stem Cell

CellPress

Short article

Epitranscriptomic regulation of cortical neurogenesis via Mettl8-dependent mitochondrial tRNA m^3C modification

Feng Zhang,[1] Kijun Yoon,[1] Daniel Y. Zhang,[1,2] Nam-Shik Kim,[1] Guo-li Ming,[1,3,4,5,7,*] and Hongjun Song[1,3,5,6,*]
[1]Department of Neuroscience and Mahoney Institute for Neurosciences, Perelman School of Medicine, University of Pennsylvania, Philadelphia, PA 19104, USA
[2]Biochemistry and Molecular Biophysics Graduate Group, Perelman School of Medicine, University of Pennsylvania, Philadelphia, PA 19104, USA
[3]Department of Cell and Developmental Biology, Perelman School of Medicine, University of Pennsylvania, Philadelphia, PA 19104, USA
[4]Department of Psychiatry, Perelman School of Medicine, University of Pennsylvania, Philadelphia, PA 19104, USA
[5]Institute for Regenerative Medicine, University of Pennsylvania, Philadelphia, PA 19104, USA
[6]The Epigenetics Institute, Perelman School of Medicine, University of Pennsylvania, Philadelphia, PA 19104, USA
[7]Lead contact
*Correspondence: gming@pennmedicine.upenn.edu (G.-l.M.), shongjun@pennmedicine.upenn.edu (H.S.)
https://doi.org/10.1016/j.stem.2023.01.007

SUMMARY

Increasing evidence implicates the critical roles of various epitranscriptomic RNA modifications in different biological processes. Methyltransferase METTL8 installs 3-methylcytosine (m^3C) modification of mitochondrial tRNAs *in vitro*; however, its role in intact biological systems is unknown. Here, we show that Mettl8 is localized in mitochondria and installs m^3C specifically on mitochondrial $tRNA^{Thr/Ser(UCN)}$ in mouse embryonic cortical neural stem cells. At molecular and cellular levels, *Mettl8* deletion in cortical neural stem cells leads to reduced mitochondrial protein translation and attenuated respiration activity. At the functional level, conditional *Mettl8* deletion in mice results in impaired embryonic cortical neural stem cell maintenance *in vivo*, which can be rescued by pharmacologically enhancing mitochondrial functions. Similarly, METTL8 promotes mitochondrial protein expression and neural stem cell maintenance in human forebrain cortical organoids. Together, our study reveals a conserved epitranscriptomic mechanism of Mettl8 and mitochondrial tRNA m^3C modification in maintaining embryonic cortical neural stem cells in mice and humans.

INTRODUCTION

The study of more than 170 chemically distinct types of RNA modifications, or epitranscriptomics, has attracted significant interest because of its critical involvement in tuning nearly every aspect of RNA biology, regulating various biological processes ranging from development to cancer, and profound successes in clinical applications of RNA modifications to improve efficacy and reduce the immunogenicity of COVID19 mRNA vaccines.[1–4] Significant progress has been made in identifying writers, erasers, and readers for different RNA modifications, which in turn provides entry points to investigate their biological functions and underlying mechanisms. Most epitranscriptomic studies have used immortal or cancer cell lines, while investigations in intact biological systems lag behind. In the mammalian nervous system, recent studies have identified diverse roles and mechanisms of epitranscriptomics, mostly focusing on mRNA m^6A modification, yet many other RNA modifications remain to be explored.[5–7]

Besides modifications on mRNA, transfer RNA (tRNA) are also heavily modified (~13 modifications/molecule) to be fully active.[8–10] Modifications of mitochondrial tRNAs (mt-tRNAs, ~5 modifications/molecule[11]) are very important for utilizing only 22 mt-tRNAs to precisely recognize 64 codons specifying 20 amino acids and stop signals and tuning mitochondria protein translation and function.[8,12] Several writers install m^3C on tRNAs.[13–17] Mettl6 is a cytosolic tRNA (cyto-tRNA) m^3C methyltransferase regulating stem cell pluripotency and tumor cell growth,[14] whereas Mettl8 is an mt-tRNA m^3C methyltransferase regulating mitochondria protein translation and activity in immortal and cancer cell lines and promoting pancreatic cancer cell growth and regulating mouse embryonic stem cell differentiation *in vitro*.[15,16,18,19] However, distinct from normal cells, metabolic reprogramming is a hallmark of immortal cell lines and cancer cells, characterized by aerobic glycolysis and enhancement of mitochondrial biogenesis,[20] and the physiological role and mechanism of Mettl8 and mt-tRNA m^3C modification in intact biological systems remain elusive. The genome-wide m^3C modification targets of Mettl8 are also unknown.

During mammalian cortical neurogenesis, neural stem cells sequentially generate deep- and superficial-layer neurons and become gradually depleted.[21] The precise timing of neurogenesis and maintenance of neural stem cells are critical for

Please cite this article in press as: Zhang et al., Epitranscriptomic regulation of cortical neurogenesis via Mettl8-dependent mitochondrial tRNA m^3C modification, Cell Stem Cell (2023), https://doi.org/10.1016/j.stem.2023.01.007

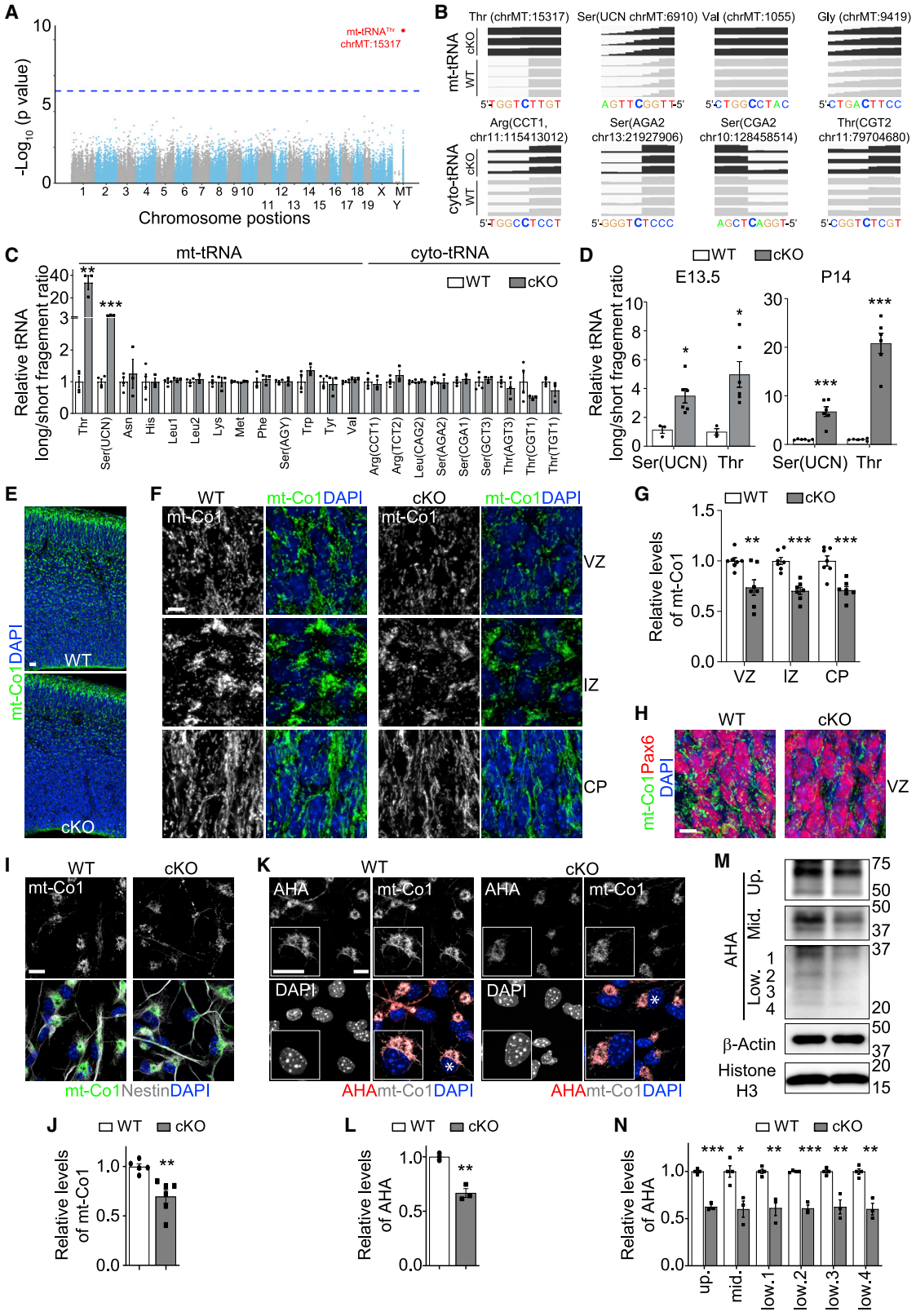

(legend on next page)

Please cite this article in press as: Zhang et al., Epitranscriptomic regulation of cortical neurogenesis via Mettl8-dependent mitochondrial tRNA m^3C modification, Cell Stem Cell (2023), https://doi.org/10.1016/j.stem.2023.01.007

producing proper numbers of neurons of different cortical layers.[22] m^6A mRNA modification is known to regulate cortical neurogenesis tempo via promoting mRNA decay[23,24] and nuclear export.[25] Mitochondria are also critically involved in regulating cortical neurogenesis through their dynamics, homeostasis, and generation of reactive oxygen species, ATP, and TCA cycle metabolites.[26–28] Here, we investigated the physiological role and mechanism of Mettl8 and mt-tRNA m^3C modification in cortical neurogenesis in mice and human induced pluripotent stem cell (iPSC)-derived forebrain organoids. We showed that *Mettl8* deletion leads to decreased m^3C modification specifically on mt-$tRNA^{Thr/Ser(UCN)}$, reduced mitochondria protein translation, and deficient mitochondrial function in cortical neural stem cells. Functionally, *Mettl8* deletion leads to accelerated depletion of cortical neural stem cells with increased neuronal differentiation, which were largely rescued by pharmacologically enhancing the respiration function of mitochondria.

RESULTS

Mettl8 installs m^3C on mt-$tRNA^{Thr/Ser(UCN)}$ in mouse embryonic cortical neural stem cells

To explore the physiological role of Mettl8 in the nervous system *in vivo*, we generated a *Mettl8*$^{flox/flox}$ (*Mettl8*$^{f/f}$) mouse line by inserting two *loxP* sites flanking the 3rd exon (92 bp) of the *Mettl8* gene, deletion of which results in a premature stop codon. We confirmed the exon 3 deletion in the *Nestin-Cre*::*Mettl8*$^{f/f}$ (cKO) mouse brain at embryonic day 13.5 (E13.5) and post-natal day 14 (P14) and in neural progenitor cells (NPCs) cultured from the E17.5 cerebral cortex of cKO mice (Figure S1A; Table S1). We found mainly one long isoform and one short splicing isoform of *Mettl8* expressed in the wild-type (WT, *Mettl8*$^{f/f}$) and cKO mouse brains (Figure S1B). We cloned both isoforms from WT and cKO brains into an expression vector with a hemagglutinin (HA) tag and found that only the long isoform from WT cDNA can be translated into a detectable protein (Figure S1C).

Mettl8 cKO mice survive into adulthood. Analysis of the P1 mouse cortex showed similar cortical thickness (Figure S1D), but more Ctip2$^+$ deep-layer neurons and fewer Cux1$^+$ superficial-layer neurons in cKO compared with WT mice, indicating aberrant cortical neurogenesis (Figures S1E–S1G).

To explore the underlying molecular mechanism, we first examined the subcellular localization of Mettl8. To overcome a lack of functional antibodies that can detect the endogenous Mettl8 protein, probably due to its low expression levels, we overexpressed mouse full-length Mettl8 and found it was co-localized with a mitochondria marker mt-Co1 (Figure S1H) and mostly in the biochemically purified mitochondria fraction (Figure S1I) from mouse neuroblastoma N2a cell lines,[29] similar to in other cell lines.[15,16,18,30] Upon *in utero* electroporation, we found co-localization of overexpressed Mettl8 protein with mt-Co1 in Pax6$^+$ neural stem cells in the ventricular zone (VZ) and in Dcx$^+$ immature neurons in the intermediate zone (IZ) in the embryonic cerebral cortex (Figures S1J–S1M).

To identify targets of m^3C modification by Mettl8, we performed hydrazine-aniline cleavage sequencing (HAC-seq)[13] using WT and cKO NPCs. Our unbiased analysis revealed Mettl8-dependent m^3C modification for only one site with genome-wide significance at the 32 position of mt-$tRNA^{Thr}$ (Figures 1A–1B; Table S2). To confirm this result, we performed an independent qPCR assay based on the blockade of reverse transcription (RT) by m^3C modification on RNA.[16] Since long and short fragments of cDNA are generated from tRNAs without and with m^3C modification during RT, respectively, we designed primer sets to specifically target these long and short fragments for qPCR and used the ratio of long fragment (unmodified) versus short fragment (unmodified + modified) levels to evaluate the m^3C modification levels of tRNAs (Figure S1N). Using WT and cKO NPCs, we examined all mt-tRNAs with Cytosine at the 32 position, with the exception of mt-$tRNA^{Gly}$ due to a lack of effective primers, and 9 cyto-tRNAs previously identified to be m^3C modified in the human breast cancer MCF7 cell line.[13] Among all tRNAs tested, mt-$tRNA^{Thr}$ and mt-$tRNA^{Ser(UCN)}$ exhibited significant Mettl8-dependent m^3C modification (Figure 1C). Careful inspection of HAC-seq data also revealed a trend of Mettl8-dependent m^3C modification for mt-$tRNA^{Ser(UCN)}$ (Figure 1B). We further confirmed Mettl8-dependent m^3C modification of mt-$tRNA^{Thr/Ser(UCN)}$ in the mouse brain at E13.5 and P14 by qPCR (Figures 1D and S1O). Together, these results indicate

Figure 1. Mettl8 installs m^3C modification of mt-$tRNA^{Thr/Ser(UCN)}$ and regulates mitochondria protein translation in mouse NPCs

(A and B) HAC-seq analysis of NPCs derived from E17.5 WT and cKO cortex. Shown are a Manhattan plot of $-\log_{10}(P)$ of the differential cleavage ratio of analyzed cytosine sites (n = 3 cKO and 4 WT) at their chromosomal positions with the blue dotted lines indicating the genome-wide significance threshold with the Bonferroni correction ($p = 0.05/135582 = 3.69 \times 10^{-7}$) (A) and alignment tracks of potential m^3C modification sites of several mt-tRNAs and cyto-tRNAs (B).

(C) qPCR measurement of the long/short ratio of 13 mt-tRNAs with a cytosine at the 32 position and 9 cyto-tRNAs previously reported to contain m^3C modifications.[13] Data were normalized to the value of WT NPCs. Values represent mean ± SEM (n = 4/WT; 3/cKO; $^{**}p < 0.01$, $^{***}p < 0.001$; Student's t test).

(D) Mettl8-dependent m^3C modification of mt-$tRNA^{Thr/Ser(UCN)}$ in E13.5 and P14 WT and cKO mouse cortex measured by qPCR. Similar as in (C). Values represent mean ± SEM (E13.5 cortex: n = 3/WT, 6/cKO; P14 cortex: n = 6/WT, 6/cKO; $^{*}p < 0.05$, $^{***}p < 0.001$; Student's t test).

(E–H) Sample confocal images of mt-Co1 immunostaining and DAPI of the E14.5 mouse cortex (E) and enlarged views for VZ, IZ, and CP regions (F), and co-immunostaining of mt-Co1 and Pax6 (H). Scale bars, 20 μm (E) and 5 μm (F and H), and quantifications of the relative intensity of the mt-Co1 signal of cKO compared with WT cortex (G). Values represent mean ± SEM (n = 7/WT, 7/cKO; $^{**}p < 0.01$, $^{***}p < 0.001$; Student's t test).

(I and J) Sample immunostaining confocal images (I; scale bar, 10 μm) and quantification of the relative intensity of the mt-Co1 signal of cKO compared with WT NPCs (J). Values represent mean ± SEM (n = 5/WT, 6/cKO; $^{**}p < 0.01$; Student's t test).

(K–N) *Mettl8* deletion attenuates mitochondria protein translation in NPCs. WT and cKO NPCs were first cultured without methionine for 1.5 h and then treated with cycloheximide (50 μg/mL) for 0.5 h, followed by methionine-depleted media containing cycloheximide and AHA (300 μM for K–L and 500 μM for M–N) for 3 h. Shown are sample confocal images (K; scale bar, 10 μm) and quantification of the relative intensity of the AHA signal in cKO compared with WT NPCs (L). Values represent mean ± SEM (n = 3/WT, 3/cKO; $^{**}p < 0.01$; Student's t test). Also shown are sample western blot images (M) and quantification of the intensity of different AHA bands (1–4 bands indicating different mitochondria proteins) normalized first with that of β-actin and then compared with WT samples (N). Values represent mean ± SEM (n = 4/WT, 3/cKO; $^{*}p < 0.05$, $^{**}p < 0.01$, $^{***}p < 0.001$; Student's t test).

See also Figures S1 and S2; Tables S1–S3

Please cite this article in press as: Zhang et al., Epitranscriptomic regulation of cortical neurogenesis via Mettl8-dependent mitochondrial tRNA m^3C modification, Cell Stem Cell (2023), https://doi.org/10.1016/j.stem.2023.01.007

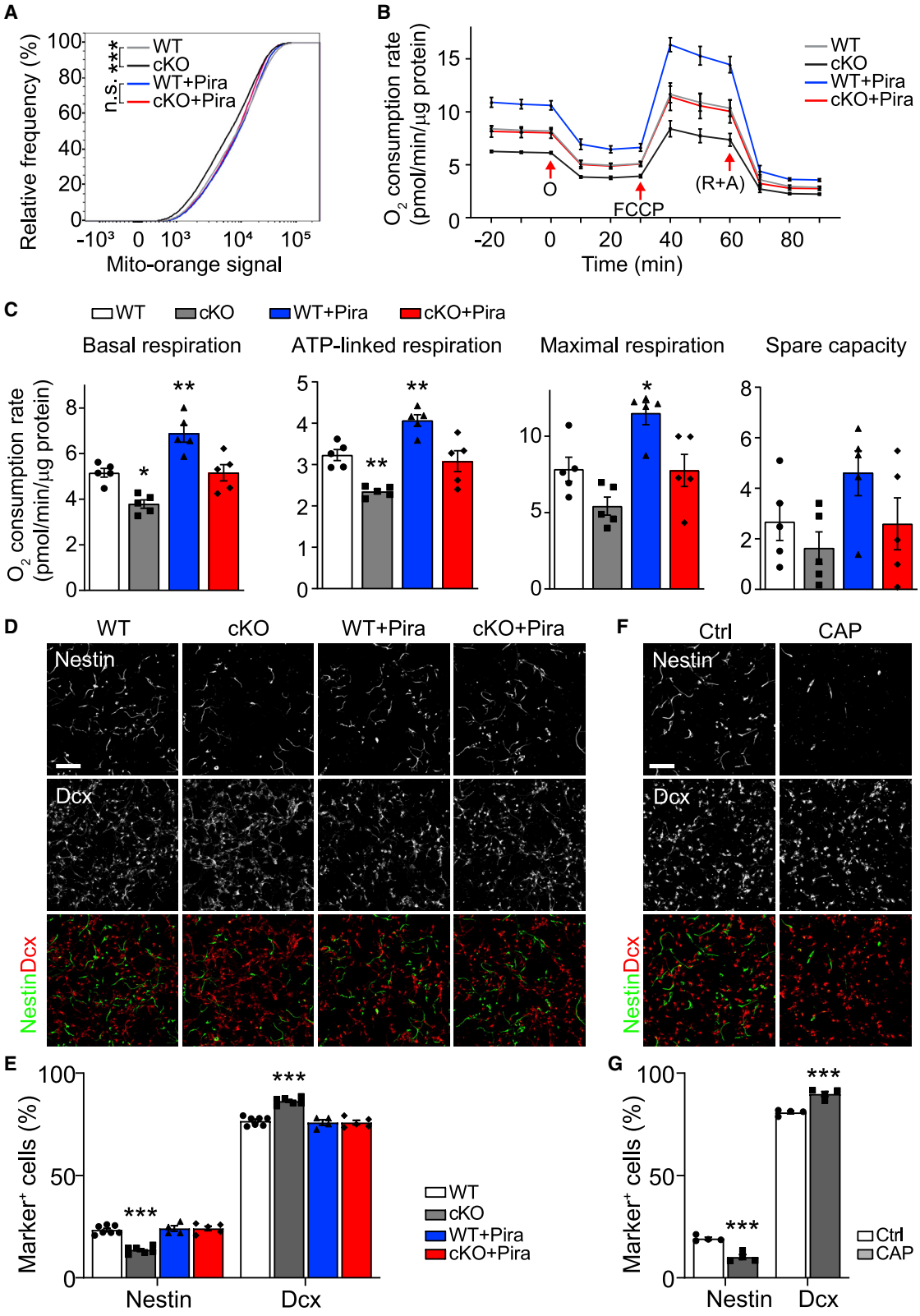

Figure 2. Mettl8 deletion attenuates mitochondria respiration activity and NPC maintenance

(A) Accumulative distributions of Mito-Orange signal levels. WT and cKO NPCs cultured with or without piracetam (Pira; 1 mM) were stained with 50 nM MMP-indicator Mito-Orange before flow cytometry analysis. The percent frequency distribution across every 400 bins of Mito-Orange signal intensity was used for quantification (number of cells analyzed: n = 48,546/WT, 49,548/KO, 50,688/WT+Pira, 53,196/KO+Pira; n.s.: $p > 0.05$, ***$p < 0.001$; Kolmogorov-Smirnov test).

(legend continued on next page)

Please cite this article in press as: Zhang et al., Epitranscriptomic regulation of cortical neurogenesis via Mettl8-dependent mitochondrial tRNA m^3C modification, Cell Stem Cell (2023), https://doi.org/10.1016/j.stem.2023.01.007

that Mettl8 is localized in mitochondrial and regulates m^3C modification levels specifically on mt-$tRNA^{Thr/Ser(UCN)}$ in mouse cortical neural stem cells.

Mettl8 regulates mitochondrial protein translation in mouse cortical neural stem cells

To explore how *Mettl8* deletion may impact neural stem cells, RNA sequencing identified 190 down- and 198 up-regulated genes in cKO compared with WT NPCs (Figure S2A; Table S3). Gene Ontology enrichment analysis of downregulated genes shows the majority of biological pathway terms related to the ATP metabolic process, oxidative phosphorylation, cellular respiration, and electron transport chain, which are closely linked to mitochondria function, and most cellular component terms related to mitochondria (Figures S2B–S2D; Table S3). Protein-protein interaction network analysis of downregulated genes also revealed pathways related to the electron transport chain and mitochondrial translation elongation process (Figure S2E; Table S3). Thus, unbiased transcriptome analysis suggests abnormal mitochondria function in cKO NPCs.

To investigate the mechanism underlying mitochondrial abnormalities in cKO NPCs, we examined mitochondrial protein translation. Immunostaining showed a decreased expression of mitochondrial genome-encoded mt-Co1 protein in different cortical layers of cKO compared with WT mice at E14.5, including $Pax6^+$ neural stem-cell-enriched VZ (Figures 1E–1H), and in cultured cKO NPCs (Figures 1I–1J). Western blot analysis showed decreased levels of mt-Co1 and mitochondrial genome-encoded mt-Co2 and mt-ATP6 proteins in the cKO E13.5 cortex and cultured NPCs compared with WT counterparts (Figures S2F–S2I). The mRNA levels of these genes were not different in the E13.5 cortex and cultured NPCs between WT and cKO samples, with the exception of a mild reduction of *mt-ATP6* mRNA levels in cKO NPCs (Figure S2J).

We specifically examined whether mitochondria protein translation is affected in NPCs using two independent assays. First, we treated cultured NPCs with chloramphenicol (CAP), a specific mitochondria protein translation inhibitor,[31] followed by a time course analysis of recovery upon inhibition release. Although CAP treatment drastically decreased mt-Co1 protein levels at 48 h, expression levels were lower in cKO compared with WT NPCs at 1.5 h and 5 h upon release from CAP treatment (Figures S2K–S2L), indicating lower levels of *de novo* translation of mt-Co1 protein in cKO NPCs. Second, we directly monitored *de novo* mitochondria protein translation in NPCs with the incorporation of methionine analog L-Azidohomoalanine (AHA).[32] Upon inhibition of cytosolic protein translation by cycloheximide,[33] the AHA signal was exclusively concentrated in mt-$Co1^+$ mitochondria (Figure 1K), indicating the specificity of this assay. Both immunostaining and western blot analyses showed attenuated levels of mitochondria incorporation of AHA in cKO compared with WT NPCs under cycloheximide treatment (Figures 1K–1N and S2M), whereas cytosolic protein translation was unaffected (Figures S2N–S2Q). Together, these results suggest that deficits of m^3C modification of mt-tRNAs lead to impaired mitochondria protein translation in mouse cKO NPCs.

Mettl8$^{-/-}$ NPCs exhibit attenuated mitochondria activity and increased differentiation

We next examined the impact of *Mettl8* deletion on the mitochondria function of NPCs. Analysis using mitochondria membrane potential (MMP)-indicator MitoTracker Orange showed a modest but significant decrease of MMP in cKO compared with WT cultured NPCs, which became insignificant upon piracetam treatment, which enhances the respiration function of mitochondria[34,35] (Figure 2A). We next performed the Seahorse assay to directly measure O_2 consumption rates and mitochondria respiration activity.[36] Levels of basal respiration and ATP-linked respiration were reduced in cKO compared with WT NPCs, whereas piracetam treatment restored them to levels comparable with WT NPCs without treatment (Figures 2B and 2C). Together, these results indicate that mitochondria function in cKO NPCs is impaired, which can be restored by piracetam treatment.

Next, we examined the impact of *Mettl8* deletion and impaired mitochondrial function on NPC properties. Under the culture condition that supports primary NPCs to either maintain the neural stem cell state or differentiate,[37] we found the percentages of $Nestin^+$ NPCs decreased and the percenatge of Dcx^+ neurons increased in cKO compared with WT samples (Figures 2D–2E). Importantly, piracetam treatment rescued these cell fate alterations in cKO samples (Figures 2D–2E). The observed effect was not due to selective cell survival (Figures S2R–S2S).

To further support that reduced mitochondria protein translation in *Mettl8* cKO NPCs is the underlying cause of impaired neural stem cell maintenance, we pharmacologically inhibited the mitochondria protein translation in primary WT NPCs by short-term CAP treatment (Figures S2T–S2U). Compared with the saline control, short-term CAP treatment led to a decreased percentage of $Nestin^+$ NPCs and an increased percentage of Dcx^+ neurons, phenocopying *Mettl8* cKO samples *in vitro* (Figures 2F and 2G).

Mettl8$^{-/-}$ mice exhibit deficits in embryonic cortical neural stem cell maintenance

We next performed *in vivo* analysis. $Pax6^+$ neural stem cells in the VZ become gradually depleted from E13.5 to E16.5 during embryonic mouse cortical development[21] (Figures 3A and 3B). We found fewer $Pax6^+$ neural stem cells, together with higher ratios of $Tbr2^+$ intermediate neural progenitors (IPCs) over $Pax6^+$ neural stem cells in the E13.5, E14.5, and E16.5 cerebral cortex of cKO compared with WT mice (Figures 3A–3C). Analysis of

(B and C) Summary of Seahorse analysis measuring O_2 consumption of WT and cKO NPCs with or without piracetam (Pira) treatment (B) and quantification of levels of basal respiration, ATP-linked respiration, maximal respiration, and spare activity (C). Values represent mean ± SEM (n = 5/WT, 5/cKO, 5/WT+Pira, 5/cKO+Pira; *$p < 0.05$; **$p < 0.01$; one-way ANOVA). O: oligomycin; (R + A): rotenone + antimycin A.
(D and E) Sample confocal images of immunostaining for Nestin and Dcx in WT and cKO primary NPCs cultured with or without piracetam (1 mM) for 48 h (D; scale bar, 100 μm) and quantification (E). Values represent mean ± SEM (n = 7/WT, 6/cKO, 4/WT+Pira, 5/cKO+Pira; ***$p < 0.001$; one-way ANOVA).
(F and G) Pharmacological inhibition of mitochondrial protein translation with CAP (10 μg/mL) for 48 h leads to similar deficits in primary NPCs as *Mettl8* deletion. Similar as in (D and E). Values represent mean ± SEM (n = 4/Ctrl, 4/CAP; ***$p < 0.001$; one-way ANOVA).
See also Figure S2

Please cite this article in press as: Zhang et al., Epitranscriptomic regulation of cortical neurogenesis via Mettl8-dependent mitochondrial tRNA m^3C modification, Cell Stem Cell (2023), https://doi.org/10.1016/j.stem.2023.01.007

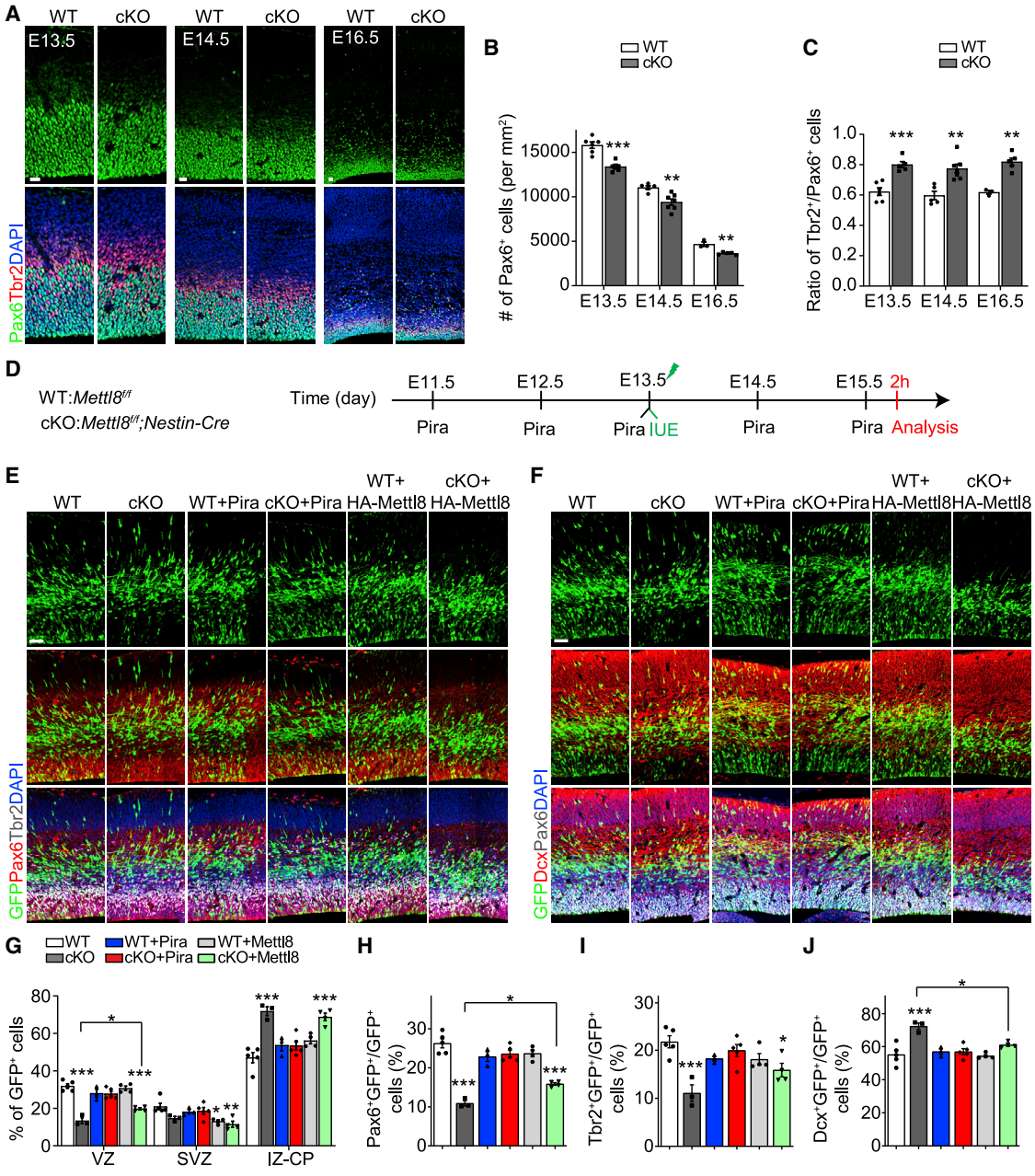

Figure 3. *Mettl8* deletion leads to deficits in cortical neural stem cell maintenance *in vivo*

(A–C) Sample immunostaining confocal images (A; scale bars, 20 μm) and quantification of the density of $Pax6^+$ neural stem cells (B) and the ratio of $Tbr2^+$ cells over $Pax6^+$ cells (C) in WT and cKO cortex. Values represent mean ± SEM (E13.5: n = 6/WT, 5/cKO; E14.5: n = 5/WT, 7/cKO; E16.5: n = 3/WT, 5/cKO; *p < 0.05, **p < 0.01, ***p < 0.001; Student's t test).

(D–J) *Mettl8* cKO mice exhibit deficits in neural stem cell maintenance with increased neuronal differentiation, which were rescued by piracetam treatment (500 mg/kg body weight). Shown are a schematic diagram of experimental design (D), sample immunostaining confocal images (E and F; scale bars, 50 μm) and quantifications for percentages of GFP^+ cells distributed across different layers of the cortex (G), and percentages of different cell types among all GFP^+ cells (H–J) in WT and cKO mice. Values represent mean ± SEM (n = 5/WT, 3/cKO, 3/WT+Pira, 5/cKO+Pira, 4/WT+Mettl8, 4/cKO+Mettl8; *p < 0.05, ***p < 0.001; one-way ANOVA).

See also Figure S3

cleaved-caspase3 expression and 2 h EdU pulsing in cKO and WT E13.5 mice indicated no differences in cell survival or proliferation (Figures S3A–S3D). Together, these results suggest that *Mettl8* deletion promotes depletion of the neural stem cell pool with increased neuronal differentiation during embryonic cortical development.

To further support this model, we injected EdU into mice at E13.5, and analysis of the distribution of EdU^+ cells across

Please cite this article in press as: Zhang et al., Epitranscriptomic regulation of cortical neurogenesis via Mettl8-dependent mitochondrial tRNA m^3C modification, Cell Stem Cell (2023), https://doi.org/10.1016/j.stem.2023.01.007

cortical layers 24 h later showed a reduced percentage of EdU^+ cells localized in the VZ and increased percentages of EdU^+Ki67^- cells and EdU^+Ctip2^+ cells among all EdU^+ cells in cKO compared with WT cortex, indicating increased cell-cycle exit and neuronal differentiation of dividing neural progenitors (Figures S3E–S3G). To specifically label neural stem cells lining the lateral ventricle surface, we performed *in utero* electroporation at E13.5 to express GFP and characterized the cell fate of GFP^+ progenies in WT and cKO mice at E15.5 (Figure 3D). The percentage of GFP^+ cells localized in the VZ was decreased, with an increase in the IZ and cortical plate (CP) in cKO compared with WT cortex (Figures 3E and 3G), consistent with the notion of decreased neural stem cells in the VZ and increased generation of neurons, which migrate to IZ and CP. Indeed, percentages of GFP^+Pax6^+ neural stem cells and GFP^+Tbr2^+ IPCs among GFP^+ cells were reduced and the percentage of GFP^+Dcx^+ immature neurons among GFP^+ cells was increased in cKO compared with WT cortex (Figures 3E–3J). Electroporation of plasmids co-expressing GFP and full-length WT Mettl8 partially rescued cellular deficits in cKO mice and the partial rescue is likely due to the time delay before the construct was highly expressed (Figures 3E–3J). Injection of piracetam, which can penetrate the placenta and blood-brain barrier,[38] from E11.5 to E15.5 also largely rescued all cellular deficits in cKO mice (Figures 3E–3J), indicating that impaired mitochondria function is the cause of deficits in neural stem cell maintenance with increased neuronal differentiation *in vivo*. Similar to Mettl8 overexpression, piracetam did not enhance neural stem cell maintenance in WT mice (Figures 3E–3J), indicating a threshold effect for Mettl8 levels and mitochondrial activities on neural stem cell maintenance.

During embryonic cortical neurogenesis, cortical neurons are sequentially generated with deep-layer neurons born first and superficial-layer neurons born later.[21] To examine the impact of *Mettl8* deletion-induced accelerated neural stem cell depletion on the generation of cortical neurons of different layers, we injected EdU into WT and cKO mice at E11.5, E13.5, and E15.5 and examined the number of neurons born at these time points by analysis of EdU^+ cells at P1. Numbers of EdU^+Ctip2^+ deep-layer neurons born at E11.5 and E13.5 were increased (Figures S3H–S3K), whereas numbers of EdU^+Satb2^+ and EdU^+Cux1^+ superficial-layer neurons born at E15.5 were decreased in cKO compared with WT mice (Figures S3L–S3O).

Together, these results show that *Mettl8* deletion leads to maintenance deficits with increased neuronal differentiation of embryonic cortical neural stem cells, resulting in excess numbers of early-born deep-layer cortical neurons and reduced numbers of later-born superficial-layer cortical neurons in mice *in vivo*.

METTL8 regulates mitochondria protein expression and maintenance of cortical neural stem cells in human forebrain organoids

Finally, we examined the role of METTL8 in human cortical neurogenesis using a human iPSC-derived forebrain organoid model[39] (Figure S4A). We generated isogenic *METTL8* knockout human iPSCs with the deletion of the third exon (92 bp) of the human *METTL8* gene, which causes a reading frameshift and premature stop codon, and we used three different clones (KO1-3 iPSCs) for our analysis. We also transfected the same founder iPSC line with a gRNA targeting the human safe harbor-*AAVS1* locus and selected four different clones as controls (WT1-4 iPSCs). We confirmed the deletion of Exon 3 of the *METTL8* gene in KO organoids at day 33 (D33, Figure S4B). qPCR analysis of the long and short fragments of cDNAs generated from mt-$tRNA^{Thr}$ and mt-$tRNA^{Ser(UCN)}$ during RT showed increased ratios in KO compared with WT organoids at D33, which were enriched with neural stem cells at this stage[39] (Figures 4A–4C). Thus, METTL8 also regulates m^3C modification of mt-$tRNA^{Thr/Ser(UCN)}$ in human cortical neural stem cells. Furthermore, immunostaining showed decreased levels of mt-CO1 in $SOX2^+$ radial glia neural stem cells localized at the VZ region of KO compared with WT organoids (Figures 4C–4D and S4C). Western blot analysis of D33 organoids also showed decreased expression levels of mt-CO2 and mt-ATP6 proteins (Figures S4D and S4E) with no change in mRNA levels (Figure S4F) in KO compared with WT organoids.

To examine the impact of *METTL8* deletion specifically on radial glia neural stem cells in forebrain organoids, we injected GFP-expressing retrovirus into the lumen of D42 organoids to specifically target dividing neural stem cells lining the lumen and permanently label their progeny for analysis of their cell fate 14 days later (Figure S4A). We found a decreased percentage of GFP^+SOX2^+ neural stem cells and an increased percentage of GFP^+CTIP2^+ neurons among all GFP^+ cells in organoids from all KO iPSC lines compared with those of all WT iPSC lines (Figures 4E–4G and S4G and S4H). Importantly, these deficits were largely rescued by long-term piracetam treatment starting from D34 (Figures 4E–4G, S4A, and S4G and S4H).

Together, these results indicate that METTL8 regulates m^3C modification of mt-tRNAs and mitochondria protein expression, and *METTL8* deletion leads to impaired maintenance of cortical neural stem cells with increased neuronal differentiation in human forebrain organoids, revealing a conserved function and mechanism of METTL8 in regulating both mouse and human brain development.

DISCUSSION

Our results support a model that Mettl8 installs m^3C on mt-$tRNA^{Thr/Ser(UCN)}$ in cortical neural stem cells to promote mitochondrial protein translation and function, which is required for maintaining neural stem cells during embryonic cortical development. Beyond previous findings of Mettl8-mediated m^3C modifications on mt-tRNAs in immortal and cancer cells,[15,16,18,30] our study reveals its physiological role and mechanism in an intact biological system *in vivo* and showed its conservation in the human brain.

Role of Mettl8 and mt-tRNA m^3C modification on mitochondrial properties and cortical neural stem cell maintenance

Using conditional brain-specific *Mettl8* knockout mouse and isogenic *METTL8* knockout human iPSC-derived forebrain organoid models, we showed that methyltransferase Mettl8 installs m^3C modification specifically on mt-$tRNA^{Thr/Ser(UCN)}$ and plays a conserved role in regulating mitochondrial protein expression and promoting neural stem cell maintenance. Our results

Please cite this article in press as: Zhang et al., Epitranscriptomic regulation of cortical neurogenesis via Mettl8-dependent mitochondrial tRNA m^3C modification, Cell Stem Cell (2023), https://doi.org/10.1016/j.stem.2023.01.007

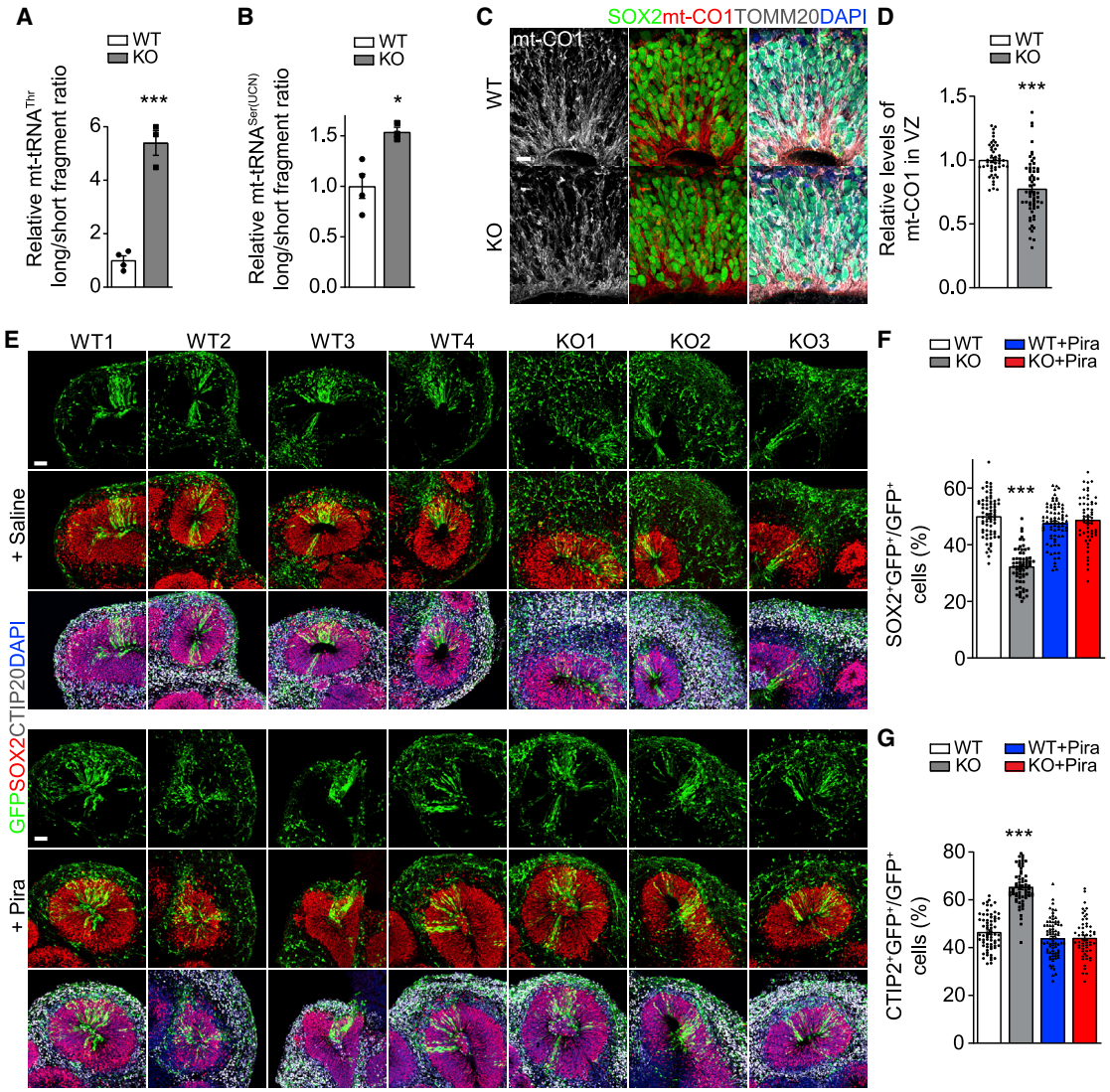

Figure 4. *METTL8* deletion reduces mitochondria protein levels and impairs radial glial neuronal stem cell maintenance in human forebrain organoids

(A and B) Reduced m^3C modification on mt-tRNA$^{Thr/Ser(UCN)}$ in day 33 (D33) *METTL8* KO organoids. Similar as in Figures 1C and 1D. Individual dots represent data from organoids derived from each iPSC line. Values represent mean ± SEM (n = 4/WT, 3/KO iPSC lines; *p < 0.05; ***p < 0.001; Student's t test).

(C and D) Sample immunostaining confocal images (C; scale bar, 10 μm) and quantification of the relative intensity of the mt-CO1 signal after normalization with the number of SOX2$^+$ neural stem cells at the VZ regions of WT and KO D33 organoids (D). Individual dots represent data from each rosette of organoids derived from either WT or KO iPSC lines. Values represent mean ± SEM (n = 48 rosettes from 4 WT iPSC lines, 61 rosettes from 3 KO iPSC lines; ***p < 0.001; Student's t test).

(E–G) Sample immunostaining confocal images (E; scale bars, 50 μm) for human forebrain organoids from each WT and KO iPSC line with or without treatment of piracetam (1 mM; from D34 to D56), injected with GFP-expressing retrovirus at D42 and analyzed 14 days later and quantification of percentages of SOX2$^+$GFP$^+$ neural stem cells (F) and CTIP2$^+$GFP$^+$ neurons (G) among all GFP$^+$ cells in WT and KO organoids at D56. values represent mean ± SEM (n = 68 sections from 4 WT iPSC lines, 64 sections from 3 KO iPSC lines, 76 sections from 4 WT iPSC lines with Pira treatment, 56 sections from 3 KO iPSC lines with Pira treatment; ***p < 0.001; one-way ANOVA).

See also Figure S4

support a model that *Mettl8* deletion shifts the cell division of NPCs from the self-renewing mode to neurogenic stem cell depletion mode during embryonic cortical neurogenesis. Importantly, the *Mettl8* deletion-induced cellular phenotypes are rescued by pharmacologically enhancing mitochondrial function, whereas short-term pharmacological reduction of mitochondrial protein translation is sufficient to mimic *Mettl8* deletion-induced cellular phenotypes. Together, these results provide a causal link from Mettl8-mediated mt-tRNA m^3C modification and mitochondrial protein translation and function to cortical neural stem cell maintenance.

Our genome-wide HAC-seq and targeted qPCR results showed Mettl8-dependent m^3C modification specifically at the position 32 of mt-tRNA^{Thr} and mt-tRNA$^{Ser(UCN)}$, but not on other

mt-tRNAs, cyto-tRNAs, or mRNA in NPCs. The m^3C modification of mt-tRNA generates an extra positive charge,[16] potentially modulating the folded structure[18] or the binding or dissociating capacity to ribosomes or proteins. About 90% of mt-$tRNA^{Thr}$ is m^3C modified based on our HAC-seq, and the molecular amount and charged percentage of mt-$tRNA^{Thr}$ are each one of the lowest among mt-tRNAs,[40] raising the possibility that m^3C modified mt-$tRNA^{Thr}$ with one extra positive charge may serve as one of the rate-limiting and tunable factors for mitochondria protein elongation.

Although stem cells were previously thought to exhibit a highly glycolytic metabolism and little to no reliance on mitochondrial OXPHOS for ATP production, mitochondrial activity, beyond just ATP generation, has been shown to play vital roles in regulating various aspects of neural stem cells, including affecting stem cell fate by intermediate metabolites from the TCA cycle and the NAD^+:NADH ratio, promoting neural stem cell differentiation by physiological ROS, and regulating neural stem cell maintenance or differentiation by mitochondria dynamics.[26–28,41]

Diverse epitranscriptomic mechanisms that regulate cortical neurogenesis

The physiological and pathological functions of Mettl8 are not well understood. Notably, m^3C has been implicated in human diseases.[42] For example, *METTL8* upregulation is associated with aggressive pancreatic cancers and lung squamous cell carcinoma,[15,43,44] and frameshift mutations in *METTL8* have been identified in colon cancers.[45] Our study reveals a critical epitranscriptomic mechanism involving mt-tRNA m^3C modification in the nervous system, specifically in regulating cortical neurogenesis, via regulating mitochondrial protein translation. Our study expands a growing list of epitranscriptomic modifications regulating mammalian cortical neurogenesis. For example, deletion of m^6A methyltransferase *Mettl14* leads to a prolonged cell cycle of radial glial neural stem cells in both mice and human forebrain organoids.[23] *Mettl14* deletion in cortical neural stem cells leads to attenuated decay,[23,24] nuclear export deficits,[25] and alternative splicing[46] of m^6A-tagged mRNA. Loss-of-function mutations in m^5C methyltransferase *Nsun2* causes microcephaly in mouse and human models.[47] NSUN2-mediated m^5C mRNA methylation promotes mRNA nuclear export[48] and may cooperate with m^6A to enhance translation of specific transcripts such as p21.[49] Mutations in *PUS7*, a tRNA and mRNA pseudouridine (Ψ) synthase, are associated with microcephaly, intellectual disability, speech delay, and aggressive behavior in multiple patients,[50,51] potentially due to dysregulated protein translation.[52] Hundreds of pre-mRNA sites are direct targets of Ψ synthases PUS1, PUS7, and RPUSD4, which regulate alternative pre-mRNA splicing.[53] Mutations of tRNA m^1G9 methyltransferase TRMT10A lead to microcephaly in humans.[54] Mutations in METTL5, which adds m^6A to 18S rRNA,[55] are associated with autosomal-recessive microcephaly and intellectual disability.[56] Together, these studies highlight diverse roles and potential mechanisms of various epitranscriptomic modifications in regulating mammalian cortical neurogenesis.

Limitations of the study

First, we presented evidence on the mitochondrial localization of Mettl8 based on overexpression, instead of the endogenous protein, due to a lack of sensitive antibodies. Our further results on deficits of specific mt-tRNA m^3C modifications, mitochondria protein translation, and properties in *Mettl8* cKO NPCs support our conclusion. Future studies with better antibodies or with a knockin tag may reveal the endogenous distribution of Mettl8 in neural stem cells. Second, our study focuses on the epitranscriptomic role of Mettl8 on neural stem cells, whereas Mettl8 also regulates m^3C modification of mt-tRNAs and mitochondrial protein expression in neurons. Therefore, Mettl8 may regulate other aspects of the nervous system, which are interesting topics for future studies with tools generated in this study.

STAR★METHODS

Detailed methods are provided in the online version of this paper and include the following:

- KEY RESOURCES TABLE
- RESOURCE AVAILABILITY
  - Lead contact
  - Materials availability
  - Data and code availability
- EXPERIMENTAL MODEL AND SUBJECT DETAILS
  - Animals
  - 2D and 3D cell cultures
- METHOD DETAILS
  - Molecular cloning and constructs
  - Tissue processing and immunostaining
  - Western blotting analysis
  - *In utero* electroporation and drug injection of mice
  - RNA extraction, m^3C modification analyses, and qPCR
  - RNA-seq, m^3C-HAC-seq, and data analysis
  - Mitochondria and cytosolic protein translation assay
  - Analysis of mitochondria membrane potential
  - Oxygen consumption rate assay
  - Generation of *METTL8* knockout human iPSCs
  - Retrovirus preparation and injection into organoids
- QUANTIFICATION AND STATISTICAL ANALYSIS

SUPPLEMENTAL INFORMATION

Supplemental information can be found online at https://doi.org/10.1016/j.stem.2023.01.007.

ACKNOWLEDGMENTS

We thank members of Ming and Song laboratories for comments and suggestions; B. Temsamrit, E. LaNoce, and A. Angelucci for laboratory support; and the Penn transgenic and chimeric mouse core for helping to generate the *Mettl8*$^{f/f}$ mice. This work was supported by grants from the National Institutes of Health (R35NS097370 and RF1MH123979 to G.-l.M. and R35NS116843 and RM1HG008935 to H.S.) and from Dr. Miriam and Sheldon G. Adelson Medical Research Foundation (to G.-l.M.).

AUTHOR CONTRIBUTIONS

F.Z. performed the majority of analyses. K.Y. and N.-S.K. generated the *Mettl8*$^{f/f}$ mice. D.Y.Z. performed HAC-seq bioinformatic analysis. F.Z., G.M., and H.S. conceived the project and wrote the manuscript with inputs from all authors.

DECLARATION OF INTERESTS

G.-l.M. is on the advisory board of *Cell Stem Cell*.

INCLUSION AND DIVERSITY

We support inclusive, diverse, and equitable conduct of research.

Received: September 12, 2022
Revised: December 7, 2022
Accepted: January 17, 2023
Published: February 9, 2023

REFERENCES

1. Helm, M., and Motorin, Y. (2017). Detecting RNA modifications in the epitranscriptome: predict and validate. Nat. Rev. Genet. *18*, 275–291. https://doi.org/10.1038/nrg.2016.169.
2. Zhao, B.S., Roundtree, I.A., and He, C. (2017). Post-transcriptional gene regulation by mRNA modifications. Nat. Rev. Mol. Cell Biol. *18*, 31–42. https://doi.org/10.1038/nrm.2016.132.
3. Morais, P., Adachi, H., and Yu, Y.T. (2021). The critical contribution of pseudouridine to mRNA COVID-19 vaccines. Front. Cell Dev. Biol. *9*, 789427. https://doi.org/10.3389/fcell.2021.789427.
4. Wiener, D., and Schwartz, S. (2021). The epitranscriptome beyond m6A. Nat. Rev. Genet. *22*, 119–131. https://doi.org/10.1038/s41576-020-00295-8.
5. Vissers, C., Sinha, A., Ming, G.L., and Song, H. (2020). The epitranscriptome in stem cell biology and neural development. Neurobiol. Dis. *146*, 105139. https://doi.org/10.1016/j.nbd.2020.105139.
6. Shafik, A.M., Allen, E.G., and Jin, P. (2020). Dynamic N6-methyladenosine RNA methylation in brain and diseases. Epigenomics *12*, 371–380. https://doi.org/10.2217/epi-2019-0260.
7. Livneh, I., Moshitch-Moshkovitz, S., Amariglio, N., Rechavi, G., and Dominissini, D. (2020). The m6A epitranscriptome: transcriptome plasticity in brain development and function. Nat. Rev. Neurosci. *21*, 36–51. https://doi.org/10.1038/s41583-019-0244-z.
8. Kirchner, S., and Ignatova, Z. (2015). Emerging roles of tRNA in adaptive translation, signalling dynamics and disease. Nat. Rev. Genet. *16*, 98–112. https://doi.org/10.1038/nrg3861.
9. Roundtree, I.A., Evans, M.E., Pan, T., and He, C. (2017). Dynamic RNA modifications in gene expression regulation. Cell *169*, 1187–1200. https://doi.org/10.1016/j.cell.2017.05.045.
10. Wellner, K., and Mörl, M. (2019). Post-transcriptional regulation of tRNA pools to govern the central dogma: A perspective. Biochemistry *58*, 299–304. https://doi.org/10.1021/acs.biochem.8b00862.
11. Pan, T. (2018). Modifications and functional genomics of human transfer RNA. Cell Res. *28*, 395–404. https://doi.org/10.1038/s41422-018-0013-y.
12. Suzuki, T., Yashiro, Y., Kikuchi, I., Ishigami, Y., Saito, H., Matsuzawa, I., Okada, S., Mito, M., Iwasaki, S., Ma, D., et al. (2020). Complete chemical structures of human mitochondrial tRNAs. Nat. Commun. *11*, 4269. https://doi.org/10.1038/s41467-020-18068-6.
13. Cui, J., Liu, Q., Sendinc, E., Shi, Y., and Gregory, R.I. (2021). Nucleotide resolution profiling of m3C RNA modification by HAC-seq. Nucleic Acids Res. *49*, e27. https://doi.org/10.1093/nar/gkaa1186.
14. Ignatova, V.V., Kaiser, S., Ho, J.S.Y., Bing, X., Stolz, P., Tan, Y.X., Lee, C.L., Gay, F.P.H., Lastres, P.R., Gerlini, R., et al. (2020). METTL6 is a tRNA m3C methyltransferase that regulates pluripotency and tumor cell growth. Sci. Adv. *6*, eaaz4551. https://doi.org/10.1126/sciadv.aaz4551.
15. Schöller, E., Marks, J., Marchand, V., Bruckmann, A., Powell, C.A., Reichold, M., Mutti, C.D., Dettmer, K., Feederle, R., Hüttelmaier, S., et al. (2021). Balancing of mitochondrial translation through METTL8-mediated m3C modification of mitochondrial tRNAs. Mol. Cell *81*, 4810–4825.e12. https://doi.org/10.1016/j.molcel.2021.10.018.
16. Kleiber, N., Lemus-Diaz, N., Stiller, C., Heinrichs, M., Mai, M.M., Hackert, P., Richter-Dennerlein, R., Höbartner, C., Bohnsack, K.E., and Bohnsack, M.T. (2022). The RNA methyltransferase METTL8 installs m3C32 in mitochondrial tRNAsThr/Ser(UCN) to optimise tRNA structure and mitochondrial translation. Nat. Commun. *13*, 209. https://doi.org/10.1038/s41467-021-27905-1.
17. Xu, L., Liu, X., Sheng, N., Oo, K.S., Liang, J., Chionh, Y.H., Xu, J., Ye, F., Gao, Y.G., Dedon, P.C., and Fu, X.Y. (2017). Three distinct 3-methylcytidine (m3C) methyltransferases modify tRNA and mRNA in mice and humans. J. Biol. Chem. *292*, 14695–14703. https://doi.org/10.1074/jbc.M117.798298.
18. Lentini, J.M., Bargabos, R., Chen, C., and Fu, D. (2022). Methyltransferase METTL8 is required for 3-methylcytosine modification in human mitochondrial tRNAs. J. Biol. Chem. *298*, 101788. https://doi.org/10.1016/j.jbc.2022.101788.
19. Gu, H., Do, D.V., Liu, X., Xu, L., Su, Y., Nah, J.M., Wong, Y., Li, Y., Sheng, N., Tilaye, G.A., et al. (2018). The STAT3 target Mettl8 regulates mouse ESC differentiation via inhibiting the JNK pathway. Stem Cell Rep. *10*, 1807–1820. https://doi.org/10.1016/j.stemcr.2018.03.022.
20. Faubert, B., Solmonson, A., and DeBerardinis, R.J. (2020). Metabolic reprogramming and cancer progression. Science *368*, eaaw5473. https://doi.org/10.1126/science.aaw5473.
21. Götz, M., and Huttner, W.B. (2005). The cell biology of neurogenesis. Nat. Rev. Mol. Cell Biol. *6*, 777–788.
22. Koo, B., Lee, K.H., Ming, G.L., Yoon, K.J., and Song, H. (2022). Setting the clock of neural progenitor cells during mammalian corticogenesis. Semin. Cell Dev. Biol. *S1084-9521*, 00170. 7. https://doi.org/10.1016/j.semcdb.2022.05.013.
23. Yoon, K.J., Ringeling, F.R., Vissers, C., Jacob, F., Pokrass, M., Jimenez-Cyrus, D., Su, Y., Kim, N.S., Zhu, Y., Zheng, L., et al. (2017). Temporal control of mammalian cortical neurogenesis by m6A methylation. Cell *171*, 877–889.e17. https://doi.org/10.1016/j.cell.2017.09.003.
24. Wang, Y., Li, Y., Yue, M., Wang, J., Kumar, S., Wechsler-Reya, R.J., Zhang, Z., Ogawa, Y., Kellis, M., Duester, G., and Zhao, J.C. (2018). N6-methyladenosine RNA modification regulates embryonic neural stem cell self-renewal through histone modifications. Nat. Neurosci. *21*, 195–206. https://doi.org/10.1038/s41593-017-0057-1.
25. Edens, B.M., Vissers, C., Su, J., Arumugam, S., Xu, Z., Shi, H., Miller, N., Rojas Ringeling, F., Ming, G.L., He, C., et al. (2019). FMRP modulates neural differentiation through m6A-dependent mRNA nuclear export. Cell Rep. *28*, 845–854.e5. https://doi.org/10.1016/j.celrep.2019.06.072.
26. Katajisto, P., Döhla, J., Chaffer, C.L., Pentinmikko, N., Marjanovic, N., Iqbal, S., Zoncu, R., Chen, W., Weinberg, R.A., and Sabatini, D.M. (2015). Stem cells. Asymmetric apportioning of aged mitochondria between daughter cells is required for stemness. Science *348*, 340–343. https://doi.org/10.1126/science.1260384.
27. Khacho, M., Harris, R., and Slack, R.S. (2019). Mitochondria as central regulators of neural stem cell fate and cognitive function. Nat. Rev. Neurosci. *20*, 34–48. https://doi.org/10.1038/s41583-018-0091-3.
28. Chakrabarty, R.P., and Chandel, N.S. (2021). Mitochondria as signaling organelles control mammalian stem cell fate. Cell Stem Cell *28*, 394–408. https://doi.org/10.1016/j.stem.2021.02.011.
29. Olmsted, J.B., Carlson, K., Klebe, R., Ruddle, F., and Rosenbaum, J. (1970). Isolation of microtubule protein from cultured mouse neuroblastoma cells. Proc. Natl. Acad. Sci. USA *65*, 129–136. https://doi.org/10.1073/pnas.65.1.129.
30. Huang, M.H., Peng, G.X., Mao, X.L., Wang, J.T., Zhou, J.B., Zhang, J.H., Chen, M., Wang, E.D., and Zhou, X.L. (2022). Molecular basis for human mitochondrial tRNA m3C modification by alternatively spliced METTL8. Nucleic Acids Res. *50*, 4012–4028. https://doi.org/10.1093/nar/gkac184.
31. Ramachandran, A., Moellering, D.R., Ceaser, E., Shiva, S., Xu, J., and Darley-Usmar, V. (2002). Inhibition of mitochondrial protein synthesis results in increased endothelial cell susceptibility to nitric oxide-induced apoptosis. Proc. Natl. Acad. Sci. USA *99*, 6643–6648. https://doi.org/10.1073/pnas.102019899.

32. Zhang, L.S., Xiong, Q.P., Peña Perez, S., Liu, C., Wei, J., Le, C., Zhang, L., Harada, B.T., Dai, Q., Feng, X., et al. (2021). ALKBH7-mediated demethylation regulates mitochondrial polycistronic RNA processing. Nat. Cell Biol. *23*, 684–691. https://doi.org/10.1038/s41556-021-00709-7.

33. Yousefi, R., Fornasiero, E.F., Cyganek, L., Montoya, J., Jakobs, S., Rizzoli, S.O., Rehling, P., and Pacheu-Grau, D. (2021). Monitoring mitochondrial translation in living cells. EMBO Rep. *22*, e51635. https://doi.org/10.15252/embr.202051635.

34. Stockburger, C., Kurz, C., Koch, K.A., Eckert, S.H., Leuner, K., and Müller, W.E. (2013). Improvement of mitochondrial function and dynamics by the metabolic enhancer piracetam. Biochem. Soc. Trans. *41*, 1331–1334. https://doi.org/10.1042/BST20130054.

35. Beckervordersandforth, R., Ebert, B., Schäffner, I., Moss, J., Fiebig, C., Shin, J., Moore, D.L., Ghosh, L., Trinchero, M.F., Stockburger, C., et al. (2017). Role of mitochondrial metabolism in the control of early lineage progression and aging phenotypes in adult hippocampal neurogenesis. Neuron *93*, 560–573.e6. https://doi.org/10.1016/j.neuron.2016.12.017.

36. Gu, X., Ma, Y., Liu, Y., and Wan, Q. (2021). Measurement of mitochondrial respiration in adherent cells by seahorse XF96 Cell Mito Stress Test. Star Protoc. *2*, 100245. https://doi.org/10.1016/j.xpro.2020.100245.

37. Zhang, F., Xu, D., Yuan, L., Sun, Y., and Xu, Z. (2014). Epigenetic regulation of Atrophin1 by lysine-specific demethylase 1 is required for cortical progenitor maintenance. Nat. Commun. *5*, 5815. https://doi.org/10.1038/ncomms6815.

38. Winblad, B. (2005). Piracetam: a review of pharmacological properties and clinical uses. CNS Drug Rev. *11*, 169–182. https://doi.org/10.1111/j.1527-3458.2005.tb00268.x.

39. Qian, X., Nguyen, H.N., Song, M.M., Hadiono, C., Ogden, S.C., Hammack, C., Yao, B., Hamersky, G.R., Jacob, F., Zhong, C., et al. (2016). Brain-region-specific organoids using mini-bioreactors for modeling ZIKV exposure. Cell *165*, 1238–1254. https://doi.org/10.1016/j.cell.2016.04.032.

40. Evans, M.E., Clark, W.C., Zheng, G., and Pan, T. (2017). Determination of tRNA aminoacylation levels by high-throughput sequencing. Nucleic Acids Res. *45*, e133. https://doi.org/10.1093/nar/gkx514.

41. Khacho, M., Clark, A., Svoboda, D.S., Azzi, J., MacLaurin, J.G., Meghaizel, C., Sesaki, H., Lagace, D.C., Germain, M., Harper, M.E., et al. (2016). Mitochondrial dynamics impacts stem cell identity and fate decisions by regulating a nuclear transcriptional program. Cell Stem Cell *19*, 232–247. https://doi.org/10.1016/j.stem.2016.04.015.

42. Bohnsack, K.E., Kleiber, N., Lemus-Diaz, N., and Bohnsack, M.T. (2022). Roles and dynamics of 3-methylcytidine in cellular RNAs. Trends Biochem. Sci. *47*, 596–608. https://doi.org/10.1016/j.tibs.2022.03.004.

43. Begik, O., Lucas, M.C., Liu, H., Ramirez, J.M., Mattick, J.S., and Novoa, E.M. (2020). Integrative analyses of the RNA modification machinery reveal tissue- and cancer-specific signatures. Genome Biol. *21*, 97. https://doi.org/10.1186/s13059-020-02009-z.

44. Tang, M., Li, Y., Luo, X., Xiao, J., Wang, J., Zeng, X., Hu, Q., Chen, X., Tan, S.J., and Hu, J. (2021). Identification of biomarkers related to CD8+ T cell infiltration with gene co-expression network in lung squamous cell carcinoma. Front. Cell Dev. Biol. *9*, 606106. https://doi.org/10.3389/fcell.2021.606106.

45. Yeon, S.Y., Jo, Y.S., Choi, E.J., Kim, M.S., Yoo, N.J., and Lee, S.H. (2018). Frameshift mutations in repeat sequences of ANK3, HACD4, TCP10L, TP53BP1, MFN1, LCMT2, RNMT, TRMT6, METTL8 and METTL16 genes in colon cancers. Pathol. Oncol. Res. *24*, 617–622. https://doi.org/10.1007/s12253-017-0287-2.

46. Ringeling, F.R., Chakraborty, S., Vissers, C., Reiman, D., Patel, A.M., Lee, K.H., Hong, A., Park, C.W., Reska, T., Gagneur, J., et al. (2022). Partitioning RNAs by length improves transcriptome reconstruction from short-read RNA-seq data. Nat. Biotechnol. *40*, 741–750. https://doi.org/10.1038/s41587-021-01136-7.

47. Flores, J.V., Cordero-Espinoza, L., Oeztuerk-Winder, F., Andersson-Rolf, A., Selmi, T., Blanco, S., Tailor, J., Dietmann, S., and Frye, M. (2017). Cytosine-5 RNA methylation regulates neural stem cell differentiation and motility. Stem Cell Rep. *8*, 112–124. https://doi.org/10.1016/j.stemcr.2016.11.014.

48. Yang, X., Yang, Y., Sun, B.F., Chen, Y.S., Xu, J.W., Lai, W.Y., Li, A., Wang, X., Bhattarai, D.P., Xiao, W., et al. (2017). 5-methylcytosine promotes mRNA export – NSUN2 as the methyltransferase and ALYREF as an m5C reader. Cell Res. *27*, 606–625. https://doi.org/10.1038/cr.2017.55.

49. Li, Q., Li, X., Tang, H., Jiang, B., Dou, Y., Gorospe, M., and Wang, W. (2017). NSUN2-mediated m5C methylation and METTL3/METTL14-mediated m6A methylation cooperatively enhance p21 translation. J. Cell. Biochem. *118*, 2587–2598. https://doi.org/10.1002/jcb.25957.

50. de Brouwer, A.P.M., Abou Jamra, R., Körtel, N., Soyris, C., Polla, D.L., Safra, M., Zisso, A., Powell, C.A., Rebelo-Guiomar, P., Dinges, N., et al. (2018). Variants in PUS7 cause intellectual disability with speech delay, microcephaly, short stature, and aggressive behavior. Am. J. Hum. Genet. *103*, 1045–1052. https://doi.org/10.1016/j.ajhg.2018.10.026.

51. Shaheen, R., Tasak, M., Maddirevula, S., Abdel-Salam, G.M.H., Sayed, I.S.M., Alazami, A.M., Al-Sheddi, T., Alobeid, E., Phizicky, E.M., and Alkuraya, F.S. (2019). PUS7 mutations impair pseudouridylation in humans and cause intellectual disability and microcephaly. Hum. Genet. *138*, 231–239. https://doi.org/10.1007/s00439-019-01980-3.

52. Han, S.T., Kim, A.C., Garcia, K., Schimmenti, L.A., Macnamara, E., Undiagnosed Diseases Network, Gahl, W.A., Malicdan, M.C., and Tifft, C.J. (2022). PUS7 deficiency in human patients causes profound neurodevelopmental phenotype by dysregulating protein translation. Mol. Genet. Metab. *135*, 221–229. https://doi.org/10.1016/j.ymgme.2022.01.103.

53. Martinez, N.M., Su, A., Burns, M.C., Nussbacher, J.K., Schaening, C., Sathe, S., Yeo, G.W., and Gilbert, W.V. (2022). Pseudouridine synthases modify human pre-mRNA co-transcriptionally and affect pre-mRNA processing. Mol. Cell *82*, 645–659.e9. https://doi.org/10.1016/j.molcel.2021.12.023.

54. Igoillo-Esteve, M., Genin, A., Lambert, N., Désir, J., Pirson, I., Abdulkarim, B., Simonis, N., Drielsma, A., Marselli, L., Marchetti, P., et al. (2013). tRNA methyltransferase homolog gene TRMT10A mutation in young onset diabetes and primary microcephaly in humans. PLoS Genet. *9*, e1003888. https://doi.org/10.1371/journal.pgen.1003888.

55. van Tran, N., Ernst, F.G.M., Hawley, B.R., Zorbas, C., Ulryck, N., Hackert, P., Bohnsack, K.E., Bohnsack, M.T., Jaffrey, S.R., Graille, M., and Lafontaine, D.L.J. (2019). The human 18S rRNA m6A methyltransferase METTL5 is stabilized by TRMT112. Nucleic Acids Res. *47*, 7719–7733. https://doi.org/10.1093/nar/gkz619.

56. Richard, E.M., Polla, D.L., Assir, M.Z., Contreras, M., Shahzad, M., Khan, A.A., Razzaq, A., Akram, J., Tarar, M.N., Blanpied, T.A., et al. (2019). Bi-allelic variants in METTL5 cause autosomal-recessive intellectual disability and microcephaly. Am. J. Hum. Genet. *105*, 869–878. https://doi.org/10.1016/j.ajhg.2019.09.007.

57. Zhang, H., Kang, E., Wang, Y., Yang, C., Yu, H., Wang, Q., Chen, Z., Zhang, C., Christian, K.M., Song, H., et al. (2016). Brain-specific Crmp2 deletion leads to neuronal development deficits and behavioural impairments in mice. Nat. Commun. *7*, 11773. https://doi.org/10.1038/ncomms11773.

58. Wen, Z., Nguyen, H.N., Guo, Z., Lalli, M.A., Wang, X., Su, Y., Kim, N.S., Yoon, K.J., Shin, J., Zhang, C., et al. (2014). Synaptic dysregulation in a human iPS cell model of mental disorders. Nature *515*, 414–418. https://doi.org/10.1038/nature13716.

59. Matsuda, T., and Cepko, C.L. (2004). Electroporation and RNA interference in the rodent retina in vivo and in vitro. Proc. Natl. Acad. Sci. USA *101*, 16–22. https://doi.org/10.1073/pnas.2235688100.

60. Ran, F.A., Hsu, P.D., Wright, J., Agarwala, V., Scott, D.A., and Zhang, F. (2013). Genome engineering using the CRISPR-Cas9 system. Nat. Protoc. *8*, 2281–2308. https://doi.org/10.1038/nprot.2013.143.

61. Love, M.I., Huber, W., and Anders, S. (2014). Moderated estimation of fold change and dispersion for RNA-seq data with DESeq2. Genome Biol. *15*, 550. https://doi.org/10.1186/s13059-014-0550-8.

62. Zhou, Y., Zhou, B., Pache, L., Chang, M., Khodabakhshi, A.H., Tanaseichuk, O., Benner, C., and Chanda, S.K. (2019). Metascape

provides a biologist-oriented resource for the analysis of systems-level datasets. Nat. Commun. *10*, 1523. https://doi.org/10.1038/s41467-019-09234-6.

63. Mi, H., Muruganujan, A., Ebert, D., Huang, X., and Thomas, P.D. (2019). PANTHER version 14: more genomes, a new Panther GO-slim and improvements in enrichment analysis tools. Nucleic Acids Res. *47*, D419–D426. https://doi.org/10.1093/nar/gky1038.

64. Dobin, A., Davis, C.A., Schlesinger, F., Drenkow, J., Zaleski, C., Jha, S., Batut, P., Chaisson, M., and Gingeras, T.R. (2013). STAR: ultrafast universal RNA-seq aligner. Bioinformatics *29*, 15–21. https://doi.org/10.1093/bioinformatics/bts635.

65. Bolger, A.M., Lohse, M., and Usadel, B. (2014). Trimmomatic: a flexible trimmer for Illumina sequence data. Bioinformatics *30*, 2114–2120. https://doi.org/10.1093/bioinformatics/btu170.

66. Tronche, F., Kellendonk, C., Kretz, O., Gass, P., Anlag, K., Orban, P.C., Bock, R., Klein, R., and Schütz, G. (1999). Disruption of the glucocorticoid receptor gene in the nervous system results in reduced anxiety. Nat. Genet. *23*, 99–103. https://doi.org/10.1038/12703.

67. Yoon, K.J., Nguyen, H.N., Ursini, G., Zhang, F., Kim, N.S., Wen, Z., Makri, G., Nauen, D., Shin, J.H., Park, Y., et al. (2014). Modeling a genetic risk for schizophrenia in iPSCs and mice reveals neural stem cell deficits associated with adherens junctions and polarity. Cell Stem Cell *15*, 79–91. https://doi.org/10.1016/j.stem.2014.05.003.

68. Chiang, C.H., Su, Y., Wen, Z., Yoritomo, N., Ross, C.A., Margolis, R.L., Song, H., and Ming, G.L. (2011). Integration-free induced pluripotent stem cells derived from schizophrenia patients with a DISC1 mutation. Mol. Psychiatry *16*, 358–360. https://doi.org/10.1038/mp.2011.13.

69. Qian, X., Su, Y., Adam, C.D., Deutschmann, A.U., Pather, S.R., Goldberg, E.M., Su, K., Li, S., Lu, L., Jacob, F., et al. (2020). Sliced human cortical organoids for modeling distinct cortical layer formation. Cell Stem Cell *26*, 766–781.e9. https://doi.org/10.1016/j.stem.2020.02.002.

70. Huang, W.K., Wong, S.Z.H., Pather, S.R., Nguyen, P.T.T., Zhang, F., Zhang, D.Y., Zhang, Z., Lu, L., Fang, W., Chen, L., et al. (2021). Generation of hypothalamic arcuate organoids from human induced pluripotent stem cells. Cell Stem Cell *28*, 1657–1670.e10. https://doi.org/10.1016/j.stem.2021.04.006.

71. Schmittgen, T.D., and Livak, K.J. (2008). Analyzing real-time PCR data by the comparative C(T) method. Nat. Protoc. *3*, 1101–1108.

72. Jacob, F., Pather, S.R., Huang, W.K., Zhang, F., Wong, S.Z.H., Zhou, H., Cubitt, B., Fan, W., Chen, C.Z., Xu, M., et al. (2020). Human pluripotent stem cell-derived neural cells and brain organoids reveal SARS-CoV-2 neurotropism predominates in choroid plexus epithelium. Cell Stem Cell *27*, 937–950.e9. https://doi.org/10.1016/j.stem.2020.09.016.

73. Ashburner, M., Ball, C.A., Blake, J.A., Botstein, D., Butler, H., Cherry, J.M., Davis, A.P., Dolinski, K., Dwight, S.S., Eppig, J.T., et al. (2000). Gene ontology: tool for the unification of biology. The Gene Ontology Consortium. Nat. Genet. *25*, 25–29. https://doi.org/10.1038/75556.

74. Ge, S., Goh, E.L., Sailor, K.A., Kitabatake, Y., Ming, G.L., and Song, H. (2006). GABA regulates synaptic integration of newly generated neurons in the adult brain. Nature *439*, 589–593. https://doi.org/10.1038/nature04404.

Please cite this article in press as: Zhang et al., Epitranscriptomic regulation of cortical neurogenesis via Mettl8-dependent mitochondrial tRNA m^3C modification, Cell Stem Cell (2023), https://doi.org/10.1016/j.stem.2023.01.007

STAR★METHODS

KEY RESOURCES TABLE

REAGENT or RESOURCE	SOURCE	IDENTIFIER
Antibodies		
Goat Polyclonal Anti-GFP	Rockland	Cat#600101215; RRID: AB_11181883
Rabbit Polyclonal Anti-Cleaved Caspase3	Cell Signaling Technology	Cat#9661; RRID: AB_2341188
Rat Polyclonal Anti-Ctip2	Abcam	Cat#ab18465; RRID: AB_2064130
Rabbit Polyclonal Anti-Cux1	Santa Cruz	Cat#sc-13024; RRID: AB_2261231
Guinea Pig Polyclonal Anti-DCX	EMD Millipore	Cat#AB2253; RRID: AB_1586992
Rabbit Monoclonal Anti-GAPDH	Cell Signaling Technology	Cat#2118; RRID: AB_561053
Rat Polyclonal Anti-HA	Roche	Cat#11867423001; RRID: AB_390918
Rabbit Polyclonal Anti-histone H3	Abcam	Cat#ab1791; RRID: AB_302613
Mouse Monoclonal Anti-Ki67	BD Biosciences	Cat#550609; RRID: AB_393778
Rabbit Polyclonal Anti-Mettl8	Abcam	Cat#ab122273; RRID: AB_11127706
Rabbit Polyclonal Anti-mt-ATP6	Sigma-Aldrich	Cat#SAB5700851;
Rabbit Polyclonal Anti-mt-ATP6	Proteintech	Cat#55313-1-AP; RRID: AB_2881305
Mouse Monoclonal Anti-mt-Co1 (Immunostaining)	Abcam	Cat#ab14705; RRID: AB_2084810
Mouse Monoclonal Anti-mt-Co1 (WB)	Thermo Fisher Scientific	Cat#459600; RRID: AB_1501840
Rabbit Polyclonal Anti-mt-Co2	Proteintech	Cat#55070-1-AP; RRID: AB_10859832
Chicken Polyclonal Anti-Nestin	Aves labs	Cat#NES; RRID: AB_2314882
Mouse Monoclonal Anti-Pax6	BD Biosciences	Cat#561462; RRID: AB_10715442
Rabbit Polyclonal Anti-Pax6	BioLegend	Cat#901301; RRID: AB_2565003
Mouse Monoclonal Anti-Satb2	Abcam	Cat#ab51502; RRID: AB_882455
Goat Polyclonal Anti-Sox2	R&D system	Cat#AF2018; RRID: AB_355110
Rabbit Monoclonal Anti-TBR2	Abcam	Cat#ab183991; RRID: AB_2721040
Rabbit Polyclonal Anti-Tomm20	THOMAS SCIENTIFIC LLC	Cat#11802-1-AP; RRID: AB_2207530
Mouse Monoclonal Anti-α-Tubulin	Cell Signaling Technology	Cat#3873S; RRID: AB_1904178
Mouse Monoclonal Anti-β-actin	Thermo Fisher Scientific	Cat#AM4302; RRID: AB_2536382
Donkey Polyclonal Anti-Goat IgG (H+L) Highly Cross-Adsorbed Secondary Antibody, Alexa Fluor 488	Thermo Fisher Scientific	Cat#A-11055; RRID: AB_2534102
Donkey Polyclonal Anti-Goat IgG (H+L) Cross-Adsorbed Secondary Antibody, Alexa Fluor 647	Thermo Fisher Scientific	Cat#A-21447; RRID: AB_2535864
Donkey Polyclonal Anti-Guinea Pig IgG (H+L) AffiniPure Secondary Antibody, Alexa Fluor 488	Jackson ImmunoResearch	Cat#706-545-148; RRID: AB_2340472
Donkey Polyclonal Anti-Guinea Pig IgG (H+L) AffiniPure Secondary Antibody, Alexa Fluor 647	Jackson ImmunoResearch	Cat#706-605-148; RRID: AB_2340476
Donkey Polyclonal Anti-Mouse IgG (H+L) Highly Cross-Adsorbed Secondary Antibody, Alexa Fluor 488	Thermo Fisher Scientific	Cat#A-21202; RRID: AB_141607
Donkey Polyclonal Anti-Mouse IgG (H+L) Highly Cross-Adsorbed Secondary Antibody, Alexa Fluor 568	Thermo Fisher Scientific	Cat#A-10037; RRID: AB_2534013
Donkey Polyclonal Anti-Rabbit IgG (H+L) Highly Cross-Adsorbed Secondary Antibody, Alexa Fluor 488	Thermo Fisher Scientific	Cat#A-21206; RRID: AB_2535792
Donkey Polyclonal Anti-Rabbit IgG (H+L) Highly Cross-Adsorbed Secondary Antibody, Alexa Fluor 568	Thermo Fisher Scientific	Cat#A-10042; RRID: AB_2534017

(*Continued on next page*)

Please cite this article in press as: Zhang et al., Epitranscriptomic regulation of cortical neurogenesis via Mettl8-dependent mitochondrial tRNA m^3C modification, Cell Stem Cell (2023), https://doi.org/10.1016/j.stem.2023.01.007

Continued

REAGENT or RESOURCE	SOURCE	IDENTIFIER
Donkey Polyclonal Anti-Rabbit IgG (H+L) Highly Cross-Adsorbed Secondary Antibody, Alexa Fluor 647	Thermo Fisher Scientific	Cat#A-31573; RRID: AB_2536183
Donkey Polyclonal Anti-Rat IgG (H+L) Highly Cross-Adsorbed Secondary Antibody, Alexa Fluor 488	Thermo Fisher Scientific	Cat#A-21208; RRID: AB_2535794
Donkey Polyclonal Anti-Chicken IgY (IgG, H+L) AffiniPure Secondary Antibody, Alexa Fluor 488	Jackson ImmunoResearch	Cat#703-545-155; RRID: AB_2340375
Anti-Mouse IgG, HRP-Linked Antibody	Cell Signaling Technology	Cat#7076, RRID: AB_330924
Anti-Rabbit IgG, HRP-Linked Antibody	Cell Signaling Technology	Cat#7074, RRID:AB_2099233
Bacterial and virus strains		
Retro-pSUBGW-U6-Ub-GFP	Zhang et al.[57]	N/A
Chemicals, peptides, and recombinant proteins		
0.05% (W/V) Trypsin-EDTA	Corning	Cat#MT25052CI
10X RT Buffer	Thermo Fisher Scientific	Cat#53032LT
2-Mercaptoethanol	Thermo Fisher Scientific	Cat#21985023
Advantage UltraPure PCR Deoxynucleotide Mix (10mM Each dNTP)	Takara Bio	Cat#639125
AMPure XP Beads	Beckman Coulter	Cat#A63880
AMV Reverse Transcriptase	Takara Bio	Cat#2630A
Aniline	THOMAS SCIENTIFIC LLC	Cat#242284
Antarctic Phosphatase	New England Biolabs	Cat#M0289S
Aqua-Mount Mounting Medium	EMSCO/FISHER	Cat#NC9428056
B-27® Supplement	Gibco	Cat#17504044
Blue Protein Loading Sample Buffer	New England Biolabs	Cat#B7703S
CHIR-99021	StemCell Technologies	Cat#72054
Chloramphenicol	Sigma-Aldrich	Cat#C0378
Chloroform	Sigma-Aldrich	Cat#C2432
cOmplete, Mini, EDTA-Free Protease Inhibitor Cocktail	Sigma-Aldrich	Cat#11836170001
Cy5 Conjugated Streptavidin	Jackson ImmunoResearch	Cat#016-170-084
DAPI	BD Biosciences	Cat#564907
DBCO-PEG4-biotin	Sigma-Aldrich	Cat#760749
DirectPCR Reagent	Fisher Scientific	Cat#NC9724951
DL-Dithiothreitol Solution	Millipore Sigma	Cat#43816
Dulbecco'S Modification of Eagle's Medium (DMEM)	Corning	Cat#10-013
Dulbecco'S Modified Eagle Medium/Nutrient Mixture F-12 (DMEM/F-12)	Gibco	Cat#11330057
Dulbecco'S Phosphate-Buffered Saline (DPBS)	Corning	Cat#14190250
EcoRI-HF Restriction Enzyme	New England Biolabs Inc	Cat#R3101S
EdU	Thermo Fisher Scientific	Cat#E10187
EZ-Tn5 Transposase	Lucigen	Cat#TNP92110
Fast Green	VWR Chemicals	Cat#E772-25G
Fast SYBR Green Master Mix	Thermo Fisher Scientific	Cat#4385612
Fetal Bovine Serum (FBS)	Corning	Cat#35-010-CV
Formaldehyde, 16%, Methanol Free, Ultra Pure	Polysciences	Cat#18814-10
Gibco DMEM, High Glucose, No Glutamine, No Methionine, No Cystine	EMSCO/FISHER	Cat#21013024
GlutaMAX Supplement	GIBCO	Cat#35050061
Heparin Solution	StemCell tech	Cat#7980

(*Continued on next page*)

Please cite this article in press as: Zhang et al., Epitranscriptomic regulation of cortical neurogenesis via Mettl8-dependent mitochondrial tRNA m^3C modification, Cell Stem Cell (2023), https://doi.org/10.1016/j.stem.2023.01.007

Continued

REAGENT or RESOURCE	SOURCE	IDENTIFIER
Hibernate A Low Fluorescence Buffer	Brain Bits	Cat#HALF100
Human EGF	Peprotech	Cat#AF-100-15
Human Insulin Solution	Sigma-Aldrich	Cat#I9278
Hydrazine	THOMAS SCIENTIFIC LLC	Cat#215155
KAPA HiFi HotStart ReadyMix	Emsco/Fisher	Cat#KK2601
KnockOut Serum Replacement	Thermo Fisher Scientific	Cat#10828028
L-Azidohomoalanine (AHA)	EMSCO/FISHER	Cat#C10102
LDN-193189	StemCell Technologies	Cat#72147
Lipofectamine 2000	Invitrogen	Cat#11668019
Lipofectamine Stem Reagent	Fisher Scientific	Cat#STEM00003
Matrigel (hESC-Qualified)	Corning	Cat#8774552
MEM Non-essential Amino Acids Solution	Gibco	Cat#11140050
MitoTracker™ Orange CMTMRos	Thermofisher scientific	Cat#M7510
mTeSR Plus	StemCell Technologies	Cat#5825
N-2 Supplement (S100X)	Thermo Fisher Scientific	Cat#17502048
Neurobasal Medium	Thermo Fisher Scientific	Cat#21103049
Not1 Restriction Enzyme	New England Biolabs Inc	Cat#R0189S
Nuclease-Free Water (Not DEPC-Treated)	Thermo Fisher Scientific	Cat#AM9937
Penicillin-Streptomycin	Thermo Fisher Scientific	Cat#15140163
PhosSTOP	Sigma-Aldrich	Cat#4906845001
Pierce™ ECL Western Blotting Substrate	Thermo Fisher Scientific	Cat#PI32109
Piracetam	Sigma-Aldrich	Cat#P5295
Polybrene	Santa Cruz	Cat#sc-134220
Poly-D-lysine	Sigma-Aldrich	Cat#P6407
Polyethylene Glycol (PEG) Solution, 40%	Sigma-Aldrich	Cat# P1458
Protease Inhibitor Cocktail	Sigma-Aldrich	Cat#P8340
Proteinase K	QIAGEN	Cat#19133
Puromycin, Dihydrochloride	EMD MILLIPORE	Cat#540411
Recombinant Human FGF-Basic	Peprotech	Cat#100-18B
ReLeSR Reagent	StemcellTech	Cat#5872
RIPA Lysis Buffer	Thermofisher	Cat#89900
RNase Inhibitor, Murine	New England Biolabs	Cat#M0314S
SB-431542	StemCell Technologies	Cat#72234
SDS (10% w/v)	Fisher Scientific	Cat#50-751-7490
Seahorse XF Media & Calibrant	Agilent	Cat#103680-100
Seahorse XFe96 FluxPak Mini	Agilent	Cat#102601
SMARTScribe Reverse Transcriptase	Takara Bio	Cat#639537
StemCell Freezing Media	ATCC	Cat#ACS-3020
StemPro Accutase Cell Dissociation Reagent	Thermo Fisher Scientific	Cat#A1110501
Streptavidin-HRP Conjugate	PerkinElmer	Cat#NEL750001EA
Sucrose	VWR Chemicals	Cat#97061-430
T4 Polynucleotide Kinase	New England Biolabs	Cat#M0289S
Target Retrieval Solution	Agilent Dako	Cat#S1699
Triton X-100	Sigma-Aldrich	Cat#T8787
Trizol Reagent	Thermo Fisher Scientific	Cat#15596026
TrypLE	Fisher scientific	Cat#12604013
Tween 20	Sigma-Aldrich	Cat#P1379
XF DMEM Medium pH 7.4	Agilent	Cat#103575
Y-27632	StemCell Technologies	Cat#72304

(*Continued on next page*)

Continued

REAGENT or RESOURCE	SOURCE	IDENTIFIER
Critical commercial assays		
Advantage 2 PCR Kit	Takara Bio	Cat#639206
Cell Fractionation Kit	Abcam	Cat#ab109719
Click-IT Plus EdU Alexa Fluor 647 Imaging Kit	Thermo Fisher Scientific	Cat#C10640
EZ-PCR Mycoplasma Test Kit	Biological Industries	Cat#2070020
KAPA Library Quantification Kit for Illumina NGS	Kapa Biosystems	Cat#KK4835
NEBNext Magnesium RNA Fragmentation Modules	New England Biolabs	Cat#E6150S
NEBNext® Multiplex Small RNA Library Prep Set for Illumina® (Set 1)	New England Biolabs	Cat#E7300S
NEBNext® rRNA Depletion Kit v2 (Human/Mouse/Rat)	New England Biolabs	Cat#E7405S
NextSeq High Output v2 75 Cycles	Illumina	Cat#20024906
Pierce™ Rapid Gold BCA Protein Assay Kit	Thermo Fisher Scientific	Cat#A53226
Qubit dsDNA HS Assay Kit	Thermo Fisher Scientific	Cat#Q33231
RNA Clean & Concentrator 5	Zymo Research	Cat#R1013
Seahorse XF Cell Mito Stress Test Kit	Agilent	Cat#103015
SuperScript III First-Strand Synthesis System	Thermo Fisher Scientific	Cat#18080051
Deposited data		
Raw and Analyzed RNA-Seq and m^3C-HAC-Seq Data	This paper	GEO: GSE214445
Code for Hac-Seq Analysis	This paper	Zenodo: https://doi.org/10.5281/zenodo.7535193
Experimental models: Cell lines		
Mouse: Neuro-2a Neuroblastoma (N2a) Cell Line	ATCC	Cat#CCL-131
Human: C1-2 iPSC Line	[58]	https://doi.org/10.1038/nature13716
Human: iPSC *METTL8*$^{-/-}$ (3 Clones)	This study	N/A
Human: iPSC *AAVS1* WT (4 Clones)	This study	N/A
Human: HEK293 Cell Line	ATCC	Cat#CRL-1573
Human: GP2-293 Cell Line	Cellosaurus	Cat#CVCL_WI48, RRID: CVCL_WI48
Experimental models: Organisms/strains		
Mouse: *Mettl8*$^{flox/flox}$	This Study	N/A
Mouse: B6.Cg-Tg(Nes-cre)1Kln/J	The Jackson Laboratory	JAX: 003771
Mouse: Crl:CD1(ICR)	Charles River Laboratory	RRID: IMSR_CRL:22
Mouse: C57BL/6	Charles River Laboratory	RRID: IMSR_CRL:27
Oligonucleotides		
The Primers and DNA Oligos Used for qPCR, Cloning and Genotyping	See Table S1	N/A
Recombinant DNA		
pCAGIG	Addgene[59]	RRID:Addgene_11159
pCAGIG/Mettl8-WT-Long	This study	N/A
pCAGIG/Mettl8-WT-Short	This study	N/A
pCAGIG/Mettl8-cKO-Long	This study	N/A
pCAGIG/Mettl8-cKO-Short	This study	N/A
pSpCas9(BB)-2A-Puro (PX459) V2.0	Addgene[60]	RRID:Addgene_62988
pSpCas9/METTL8-Upstream	This study	N/A
pSpCas9/METTL8-Downstream	This study	N/A
pSpCas9/AAVS1	This study	N/A
Retro-X™ Universal Packaging System with pVSV-G	Clontech	Cat#631530

(*Continued on next page*)

Please cite this article in press as: Zhang et al., Epitranscriptomic regulation of cortical neurogenesis via Mettl8-dependent mitochondrial tRNA m^3C modification, Cell Stem Cell (2023), https://doi.org/10.1016/j.stem.2023.01.007

Continued

REAGENT or RESOURCE	SOURCE	IDENTIFIER
pSUBGW Vector	[57]	N/A
Software and algorithms		
Adobe Illustrator CC	Adobe	https://www.adobe.com/products/illustrator.html; RRID: SCR_010279
Adobe Photoshop CC	Adobe	https://www.adobe.com/products/photoshop.html; RRID: SCR_014199
Bcl2fastq v2.17.1.14	Illumina	https://support.illumina.com/sequencing/sequencing_software/bcl2fastq-conversion-software.html; RRID: SCR_015058
DESeq2 v1.36.0	[61]	https://bioconductor.org/packages/release/bioc/html/DESeq2.html; RRID:SCR_015687
FlowJo	FlowJo	https://www.flowjo.com/solutions/flowjo; RRID: SCR_008520
GraphPad Prism	GraphPad Software	https://www.graphpad.com/scientific-software/prism/; RRID: SCR_002798
ImageJ	NIH	https://imagej.nih.gov/ij/; RRID: SCR_003070
Imaris	Bitplane	https://imaris.oxinst.com/packages;RRID:SCR_007370
Metascape	[62]	http://metascape.org/gp/index.html#/main/step1; RRID: SCR_016620
Panther v15.0	[63]	http://www.pantherdb.org/; RRID: SCR_004869
R Project v3.6.0	Open source	https://www.r-project.org/; RRID: SCR_001905
RStudio v1.2.1335	Open source	https://rstudio.com/; RRID: SCR_000432
STAR v2.5.2A	[64]	https://github.com/alexdobin/STAR; RRID: SCR_015899
Trimmomatic v0.32	[65]	http://www.usadellab.org/cms/index.php?page=trimmomatic; RRID:SCR_011848
Other		
4%–20% Mini-Gel 15-Well,	BIO-RAD	Cat#4561096
6-Well Ultra-Low Attachment Culture Plate	Fisher Scientific	Cat#7200601
Amersham Imager 600	GE healthcare	N/A
Charged Microscope Slides	Fisher Scientific	Cat#22-035813
Corning 96-Well Clear Ultra Low Attachment Microplates	Corning/NETA	Cat#7201680
Forma Steri-Cult CO2 Incubator	Thermo Fisher Scientific	3310
LSR II Flow Cytometer	BD Biosciences	N/A
MaxQ CO2 Plus Shaker	Thermo Fisher Scientific	88881102
NextSeq550	Illumina	SY-415-1002
PCR Tube Strips	Emsco/Fisher	Cat#AB0490
Qubit 3 Fluorimeter	Thermo Fisher Scientific	Cat#Q33216
Seahorse XFe96 Analyzer	Agilent	N/A
StepOnePlus Real-Time PCR	Applied Biosystems	4376592
TB Syringe (26 G x 3/8 in, 1 ml)	BD Biosciences	Cat#309625

(*Continued on next page*)

Please cite this article in press as: Zhang et al., Epitranscriptomic regulation of cortical neurogenesis via Mettl8-dependent mitochondrial tRNA m^3C modification, Cell Stem Cell (2023), https://doi.org/10.1016/j.stem.2023.01.007

Continued

REAGENT or RESOURCE	SOURCE	IDENTIFIER
Trans-Blot Turbo Mini 0.2 um PVDF Transfer Packs	BIO-RAD	Cat#1704156
Scanning Confocal Microscope	Carl Zeiss	Zeiss LSM 780

RESOURCE AVAILABILITY

Lead contact

Further information and requests for resources and reagents should be directed to and will be fulfilled by the lead contact, Dr. Guo-li Ming (gming@pennmedicine.upenn.edu).

Materials availability

All unique/stable reagents and biological material generated in this study are available from the lead contact, Dr. Guo-li Ming (gming@pennmedicine.upenn.edu), with a completed materials transfer agreement.

Data and code availability

- The RNA-seq and HAC-seq data reported in this study are deposited in NCBI GEO: GSE214445.
- The code for HAC-seq analysis can be found at Zenodo: https://doi.org/10.5281/zenodo.7535193, which is maintained by Dr. Daniel Y. Zhang.
- Any additional information required to reanalyze the data reported in this paper is available from the lead contact upon request.

EXPERIMENTAL MODEL AND SUBJECT DETAILS

Animals

All experimental procedures with mice used in this study were performed in accordance with protocols approved by the Institutional Animal Care and Use Committee of University of Pennsylvania. All mice were kept in cages with bedding materials and housed in a 14-hour light/10-hour dark cycle with regular food and water changes. C57BL/6 mice and pregnant CD1 mice at E17.5 were purchased from Charles River Laboratories. *Mettl8*$^{f/f}$ mice, with insertion of two loxp sites flanking the 3rd exon (92 bp) of the *Mettl8* gene, were constructed through CRISPR/Cas9 mediated homologous recombination by injecting the mixture of Cas9 protein/gRNA/donor DNA into fertilized eggs. The *Mettl8*$^{f/f}$ mice used in this study were backcrossed for at least four generations and maintained on a C57BL/6 background. *Nestin-Cre* (B6.Cg-Tg$^{(Nes\text{-}cre)1Kln}$/J) transgenic mice were purchased from the Jackson Laboratory.[66] *Nestin-Cre*::*Mettl8*$^{f/f}$ mice (cKO mice) were used as brain-specific conditional knockout mice with littermates *Mettl8*$^{f/f}$ (WT) mice as controls. For all of experiments involving mice at embryonic stages and P1, both male and female mice were used, and no obvious sex differences were observed in experiments performed in this study. The primers used for genotyping were listed in Table S1.

2D and 3D cell cultures

Neuroblastoma (N2a) cells, HEK293 and GP2-293 Packaging Cell Line (Cellosaurus) were cultured in DMEM (Corning) with 10% fetal bovine serum (FBS, Corning) and 1% penicillin/streptomycin (P/S, Gibco), and routinely passaged every three days after digestion by 0.05% (W/V) Trypsin-EDTA (Corning) for 3–5 mins. pCAGIG-GFP/HA-Mettl8 (full-length) plasmids were transfected into N2a cells or HEK293 cells with Lipo2000 (Invitrogen).

For primary NPC cultures, WT or *Mettl8* cKO or CD1 mouse cerebral cortex at E17.5 were dissected and digested with trypsin-EDTA at 37°C for 15 mins, and then dissociated into single cells. Primary NPCs were cultured (10^5/well) in plates pre-coated with 1% Matrigel and in the DMEM/F12 medium containing 2% B27 supplement, 1% N2 supplement, bFGF (20 ng/mL), EGF (20 ng/mL), 1% GlutaMAX, 1% P/S with digestion using Accutase (ThermoFisher) for passaging. For analysis of neural stem cell maintenance, freshly dissected primary NPCs were seeded ($2x10^5$/well) on plates pre-coated with 20 ng/mL poly-D-lysine (pdL) and cultured first in DMEM/10% FBS/1% P/S for 2 hours and then in the DMEM/F12 medium containing 1% N2 supplement, bFGF (20 ng/mL), 1% GlutaMAX, 1% P/S for 48 hours.[37]

The founder human iPSC line (C1-2) used in the current study was previously generated from male neonatal foreskin fibroblasts from ATCC (CRL-2097) and fully characterized.[58,67–69] Generation of iPSC lines followed institutional IRB and ISCRO guidelines and was approved by Johns Hopkins University School of Medicine. All studies related with human iPSCs were performed in accordance with approved protocols of the University of Pennsylvania. Human iPSCs were cultured in the hESC-qualified Matrigel-coated plates in a feeder-free way and maintained in mTeSR plus medium (StemcellTech), with culture medium replaced every day. For passaging every week, iPSCs were incubated with ReLeSR reagent (StemcellTech) for 3–5 mins, and detached iPSC clumps were broken into smaller clusters by gentle trituration using 1 mL pipette tips and then were seeded onto freshly coated plates.

C1-2 iPSC lines were confirmed to have a normal karyotype and tested negative for Mycoplasma, Acholeplasma, and Spiroplasma using EZ-PCR™ Mycoplasma Detection Kit (Biological Industries).

Generation of forebrain organoids was performed as described previously with minor modification.[39,70] Briefly, iPSCs were detached by incubation with ReLeSR reagent for 3–5 mins, transferred to an ultra-low Attachment U-bottom 96-well plates (50K cells/well) and cultured in mTeSR plus media supplemented with 10 μM Y-27632 (StemcellTech) for 2 days for Embryoid Body (EB) aggregation. On Day 3–7, EBs were transferred to an ultra-low Attachment 6-well plate (Corning Costar) and cultured in H1 neural induction medium containing DMEM/F12 supplemented with 20% KnockOut Serum Replacement, 1% P/S, 1% MEM-NEAAs, 1% GlutaMAX, 0.1 mM 2-mercaptoethanol, 0.0002% heparin, 5 μM SB-431542 (StemcellTech) and 1 μM LDN-193189 (StemcellTech). On Day 6, half of the medium was replaced with F2 forebrain induction medium containing DMEM/F12 supplemented with 1% N2 supplement, 1% P/S, 1% MEM-NEAAs, 1% GlutaMAX, 0.1 mM 2-mercaptoethanol, 1 μM SB-431542, and 1 μM CHIR99021 (StemcellTech). On Day 7, organoids were embedded in Matrigel and cultured in F2 medium for 7 days. On Day 14, embedded organoids were dissociated from Matrigel by gentle pipetting, transferred to an ultra-low Attachment 6-well plate placing on a CO_2 resistant orbital shaker (ThermoFisher) and cultured in H3 differentiation medium containing DMEM/F12 supplemented with 1% B27 supplement, 2% N2 supplement, 1% P/S, 1% MEM-NEAAs, 1% GlutaMAX, 0.1 mM 2-mercaptoethanol, and 3 mg/L human insulin (Sigma).

For mitochondria protein translation inhibition or piracetam rescue experiments, mouse NPCs or human forebrain organoids were treated with 10 μg/mL chloramphenicol (CAP, Sigma) dissolved in ethanol or 1 mM piracetam dissolved in PBS, respectively. For treatment of brain organoids with piracetam, H3 medium containing piracetam was changed every 48 hours.

METHOD DETAILS

Molecular cloning and constructs

Both the long and short isoforms of *Mettl8* were amplified by PCR from complementary DNA (cDNA) of WT and cKO mouse brains at P14 and cloned into the pCAGIG plasmids with a C-terminal HA tag[59] (Addgene plasmid #11159). Paired gRNAs targeting the 2nd intron and 3rd intron of human *METTL8*, respectively, or gRNAs targeting human *AAVS1* locus were designed by Benchling website (https://www.benchling.com/), and the corresponding DNA oligonucleotides were annealed and ligated with BbsI digested pSpCas9(BB)-2A-Puro plasmids (PX459, Addgene plasmid #62988), which express Cas9 protein, gRNA and are puromycin resistant.[60] The sequences of these plasmids were verified by Sanger sequencing. The sequences of primers used for *Mettl8* cloning and DNA oligonucleotides of gRNA are listed in Table S1.

Tissue processing and immunostaining

NPCs or N2a cells were fixed with 4% paraformaldehyde (PFA) at room temperature for 30 mins, and immersed in PBS at 4°C. For tissue histology, the mice were first perfused with ice-cold PBS for 10 mins, followed by ice-cold 4% PFA for 5 mins. Dissected mouse brains were fixed in 4% PFA at 4°C overnight and then dehydrated in 30% sucrose in PBS at 4°C for 48 hours. Coronal brain serial sections at 30 μm thickness were sequentially attached on 5 slides using a cryostat (Leica, CM3050S) or a sliding microtome (Leica, SM2010R). Forebrain organoids were first fixed in 4% PFA at room temperature for 1 hour and dehydrated in 30% sucrose at 4°C overnight.

When antigen retrieval was necessary for some antibodies, brain or organoid sections were incubated in 1x Target Retrieval Solution (Agilent Dako) at 95°C for 10 mins, followed by cooling to room temperature. For immunostaining, sections or fixed cells were first washed in the blocking buffer (5% BSA, 10% FBS, 0.3% Triton X-100, 0.01% NaN_3 dissolved in PBS) at room temperature for 1 hour, and then incubated in the primary antibody diluted in the blocking buffer at 4°C overnight. After washes in PBS for 3x10 mins, the sections or cells were incubated in the Alexa Fluor 488, 568, 647 (Jackson ImmunoResearch or Invitrogen)-conjugated secondary antibodies (1:500) and DAPI (Roche, 1:500) diluted in the blocking buffer at room temperature for 1–2 hours. After a second round of washing with PBS, the sections or cells were mounted with Aqua-Mount Mounting Medium (EMSCO/Fisher). EdU staining was performed by following the manufacturer's instructions of Click-iT EdU Alexa Fluor 647 Imaging Kit (EMSCO/FISHER) after secondary antibody staining. The antibodies used for immunostaining were listed in the Key Resource Table. The confocal images with multiple z stacks were acquired by Zeiss LSM810 confocal microscopy with 20X, 40X or 63x objectives.

Western blotting analysis

Different fractions, including whole cell lysates (W), nucleus (N), mitochondria (M) and cytosol (C), of N2a cells were separated with Cell Fractionation Kit (Abcam) following the manufacturer's instructions. Briefly, N2a cells were collected and suspended in 1x buffer A to 6.6 x 10^6 cells/ml. Then equal volume of Buffer B was added, incubated for 7 mins on a rotator at room temperature and subjected to centrifugation at 5,000 x g for 1 min at 4°C. The supernatant would be the cytosol fractions (C), and the resulting pellet was suspended with 1x Buffer A. The resuspended sample was added with equal volume of Buffer C, incubated for 10 minutes on a rotator at room temperature and subjected to centrifugation at 5,000 x g for 1 min at 4°C. The supernatant would be the mitochondria fractions (M), and the resulting pellet was suspended with 1x Buffer A, which would be the nuclear fractions (N).

Protein lysates of whole cells, cells fractions, mouse brain, or human forebrain organoids were prepared in the cell lysis buffer including RIPA lysis buffer (Thermofisher), phosphatase Inhibitor Mixture (Sigma), and protease Inhibitor Mixture (Sigma). After the protein concentration was determined by Pierce™ Rapid Gold BCA Protein Assay Kit, protein lysates were denatured in 1x Sample

Please cite this article in press as: Zhang et al., Epitranscriptomic regulation of cortical neurogenesis via Mettl8-dependent mitochondrial tRNA m^3C modification, Cell Stem Cell (2023), https://doi.org/10.1016/j.stem.2023.01.007

buffer (NEB) and boiled at 95°C for 10 mins. Then ~25 μg of protein was loaded on a 4%–20% Mini-Gel (Bio-Rad), separated through SDS/PAGE and transferred into the Trans-Blot Turbo 0.2 μm PVDF membrane (Bio-Rad). After soaking PVDF membranes in 5% milk dissolved in TBS (20 mM Tris·HCl pH 8.0, 50 mM NaCl) at room temperature for 2 hours, the membranes were incubated in primary antibodies diluted in the blocking buffer (TBS, 0.1% Tween-20, 5% BSA, 0.01% NaN_3) at 4°C overnight and subsequently in the secondary antibodies conjugated with horseradish peroxidase (HRP) diluted in the blocking buffer at room temperature for 1–2 hours. Finally, Pierce™ ECL Western blotting Substrate (EMSCO/FISHER) was used for visualization of the corresponding protein bands on membranes. The antibodies used for WB were listed in the Key Resource Table.

In utero electroporation and drug injection of mice

A stock solution of 10 mg/mL EdU (ThermoFisher) was prepared in PBS and incubated on a shaker at 37°C until fully dissolved. For the EdU labeling experiment, WT and *Mettl8* cKO mice at E11.5, E13.5 or E15.5 were intraperitoneally injected with EdU (16.7 mg/kg) once and dissected 24 hours later or at P1.

In utero electroporation was performed as described previously.[37] Briefly, 2 μg/μL pCAGIG-GFP or pCAGIG-HA-Mettl8 (expressing long isoform of WT *Mettl8*) plasmids mixed with FastGreen (Sigma-Aldrich, F7252) were injected into the lateral ventricle of WT and cKO brains at E13.5 with a calibrated glass micropipette powered by an air pump. These brains were then given an electrical stimulation (50 V for 50 ms with a 950 ms interval) for 5 times and collected at E15.5. For piracetam rescue experiment, piracetam (Sigma-Aldrich, P5295) was dissolved in PBS (100 mg/mL) and injected intraperitoneally into WT and cKO mice (500 mg/Kg) once a day from E11.5 to E15.5.

RNA extraction, m^3C modification analyses, and qPCR

RNA extraction and qPCR analysis was performed as described previously.[71] Briefly, the brain tissue, cell culture or human organoids were homogenized and dissolved in 1 mL Trizol (Invitrogen) for 15 mins on ice and 200 μL chloroform was subsequently added. After centrifugation at 12000 g for 15 mins at 4°C, about 400 μL supernatant was carefully taken out and mixed with the same volume of ethanol, and the mixture was transferred to Zymo-Spin™ IC Column in a Collection Tube from the kit of Zymo RNA Clean & Concentrator™-5. After centrifugation, 400 μL RNA Prep buffer, 700 μL RNA Wash buffer and 400 μL RNA Wash buffer was sequentially added to the column with each procedure followed by centrifugation. Finally, about 15 μL RNase/DNase-free water was added to elute the column to collect the RNA sample. Subsequently, about 0.5–1 μg RNA was used for reverse transcription (RT) to synthesize the cDNA with poly-dT primers following the manufacturer's instructions of SuperScript III First-Strand Synthesis System (Invitrogen).

m^3C-HAC-seq was performed as described previously with minor modifications, based on the finding that the hydrazine treatment, followed by subsequent aniline treatment, could specifically induce the cleavage of RNA chain at the m^3C modification sites.[13] 8 μg total RNA was fragmented by incubating in 20 μl of RNA fragmentation reagents (NEB, E6150S) at 95°C for 4 mins. The fragmentation reaction was stopped by adding 2 μl 10x RNA Fragmentation Stop Solution. Then 0.1 volume NaAc (3M, pH 5.2) and 3 volumes of cold ethanol was added for ethanol precipitation of RNA. The collected RNA fragments were dephosphorylated with Antarctic phosphatase (NEB) and re-phosphorylated with T4 PNK (NEB) following the manufacturer's protocols for end repair, and then RNA was purified with the Zymo RNA-Clean&Concentrator-5 kit. Then RNA samples were incubated with 50 μl of ice-cold hydrazine buffer (10% hydrazine, 3M NaCl) on ice in the dark for 4 hours, which was stopped by ethanol precipitation. Next, RNA pellet was resuspended in 200 μl cleavage buffer (H_2O:glacial acid:aniline = 7:3:1) and incubated at room temperature in the dark for 2 hours. RNA was then ethanol precipitated and dissolved in nuclease-free water, followed by rRNA depletion with NEBNext rRNA Depletion Kit (NEB, E7400). Lastly, 100 ng of ribominus RNA fragments were used for cDNA library preparation with the NEBNext Small RNA Library Prep Set (NEB, E7300) following the manufacturer's protocol. Different libraries from 4 WT and 3 cKO NPCs were quantified using KAPA library Quantification kit and pooled together at equal molar amounts. The average fragment size of the final library fragment was determined as ~222 bp by using bioanalyzer (Agilent). About 2.7 pmol DNA was loaded on NextSeq high output kit (75 cycles, Illumina) and subjected to a NextSeq 550 sequencer (Illumina) and 1x75 bp single-end sequencing was performed to an average depth of 40 million reads per sample.

For detection of m^3C modification of mt-tRNAs and cyto-tRNAs by q-PCR, tRNA RT primers that have the reverse complement sequence of 3′ fragment of tRNA plus one 72-bp fragment of GFP were used to capture tRNA during RT reaction, respectively. For RT, about 0.5–1 μg RNA, 0.5 μL of mt-tRNA RT primer (2 mM) and 0.5 μL dNTP mixture (10 mM each) were mixed in total 5 μL of reaction system and incubated at 65°C for 5 mins. Then 2 μL of $MgCl_2$ (25 mM), 1 μL of DTT (1 mM), 1 μL of 10x RT Buffer (Invitrogen, 53032LT), 0.5 μL of RNase Inhibitor (40U/μL, NEB) and 0.5 μL of AMV reverse transcriptase (Takara) were mixed, and incubated at 50°C for 50 mins and 85°C for 5 mins. For qPCR reactions, 6 μL of H_2O, 1 μL of forward primer (10 mM), 1 μL of reverse primer (10 mM),10 μL of Fast SYBR Green qPCR Master Mix (ThermoFisher) and 2 μL of 1:5 diluted cDNA generated by poly-dT or tRNA RT primers were mixed. Then qPCR reactions were performed on the StepOnePlus Real-Time PCR System (Applied Biosystems) with thermocycling conditions as follows: 95°C for 20 s, 44 cycles of 95°C for 3 s and 60°C for 30 s. The difference value between the CT values (ΔCt) of the genes of interest and internal control genes was calculated and $2^{(-\Delta\Delta Ct)}$ was used to calculate the fold-change in expression of the genes between two samples. For qPCR measuring the level of m^3C modification of mt-/cyto-tRNAs, short primer sets can detect both long and short fragments, and long primer sets can only detect long fragment of mt-/cyto-tRNA cDNA generated from mt-/cyto-tRNAs without m^3C modification in RT. The long/short ratio, indicated by the value of $2^{(\text{the difference of CT values from qPCR when using short and long primer sets})}$, reflects the m^3C modification level. The higher the long/short value, the lower the m^3C modification level. The primers used in qPCR and RT are listed in Table S1.

RNA-seq, m^3C-HAC-seq, and data analysis

RNA-seq libraries of WT and cKO NPCs were prepared based on the SMART-seq2 method as previously described with minor modifications.[72] In brief, for RT, 3.2 μL RNA (100 ng/μL), 0.25 μL RNase inhibitor (NEB) and 1 μL CDS primer (10 μM, 5′-AAGCAGTGG TATCAACGCAGAGTACT30VN-3′) were mixed in an 8-well PCR tube strip and incubated at 70°C for 2 mins. Then, 2 μL of 5x SMARTScribe RT Buffer (TaKaRa), 0.5 μL of DTT (100 mM), 0.3 μL of $MgCl_2$ (200 mM), 1 μL of dNTPs (10 mM), 1 μL of TSO primer (10 μM, 5′-AAGCAGTGGTATCAACGCAGAGTACATrGrGrG-3′), 0.25 μL of RNase inhibitor (NEB), and 0.5 μL SMARTScribe reverse transcriptase (TaKaRa) was added. RT was performed at 42°C for 90 mins, followed by 10 cycles of 50°C for 2 mins and 42°C for 2 mins, and then 70°C for 15 mins. To amplify the full-length cDNA, 2 μL of the RT reaction, 2.5 μL of 10x Advantage 2 buffer (TaKaRa), 2.5 μL of dNTPs (2.5 mM), 0.25 μL of IS PCR primer (10 μM, 5′-AAGCAGTGGTATCAACGCAGAGT-3′), 0.5 μL Advantage DNA Polymerase (TaKaRa) and 17.25 μL nuclease-free water were mixed, and thermocycling conditions of PCR were as follows: 94°C for 3 mins, 8 cycles of 94°C for 15 s, 65°C for 30 s, and 68°C for 6 mins, followed by 72°C for 10 mins, and 4°C indefinitely. PCR products were then purified with 0.8x AMPure XP beads (Beckman Coulter), eluted in nuclease-free water and quantified following the instructions of Qubit dsDNA HS assay kit (ThermoFisher). For tagmentation of cDNA, 2 μL cDNA (50 pg/μL), 2.5 μL 2x TD buffer (20 mM Tris/pH 8.0, 10 mM $MgCl_2$, and 16% PEG 8000) and 0.5 μL adaptor-loaded Tn5 transposase (Lucigen) were mixed and incubated at 55°C for 12 mins. Then the reaction was terminated by adding 1.25 μL of 0.2% SDS (Fisher) and incubated at room temperature for 10 mins. PCR reaction was performed after addition of 16.75 μL H_2O, 1 μL of Nextera i7 primer (10 mM), 1 μL of Nextera i5 primer (10 mM), and 25 μL KAPA HiFi HotStart ReadyMix (EMSCO/FISHER), with the thermocycling conditions as follows: 72°C for 5 min, 95°C for 1 minute, 14 cycles of 95°C for 30 s, 55°C for 30 s, and 72°C for 30 s, followed by 72°C for 1 minute, and 4°C indefinitely. PCR products were then purified twice with 0.8x AMPure XP beads, eluted in nuclease-free water, and quantified following the instructions of Qubit dsDNA HS assay kit. Different libraries from 6 WT and 6 cKO NPCs were quantified using KAPA library Quantification kit and pooled together at equal molar amounts. The average fragment size of the final library fragment was determined as ~420 bp by using a bioanalyzer (Agilent), and the concentration of the library was determined by qPCR. About 2.7 pmol DNA was loaded on NextSeq high output kit (75 cycles, Illumina) and subjected to a NextSeq 550 sequencer (Illumina) and 1x58 bp single-end sequencing was performed to an average depth of 10 million reads per sample.

Raw sequencing data from RNA-seq and m^3C-HAC-seq were demultiplexed with bcl2fastq2 v2.17.1.14 (Illumina), and adaptors were trimmed using Trimmomatic v0.32 software with MINLEN setting as 18 and 26, respectively.[65] Alignments were made using STAR v2.5.2a to GENCODE mouse reference genome GRCm38.p6.[64] For m^3C-seq analysis, all cytosine sites were analyzed when their +1 bp downstream sites were a) within genomic regions with known features including genes and tRNAs, b) at the start end of more than one read in each WT sample, and c) with coverage in all samples. The cleavage ratio of $site_i$ was calculated as the ratio of the number of reads starting at $site_{i+1}$ to the read depth of $site_{i+1}$. The cleavage ratio of all analyzed 135582 cytosine sites are listed in Table S2. The genome-wide significance was determined with Bonferroni correction ($p = 0.05/135582 = 3.69\times10^{-7}$). For RNA-seq analysis, only uniquely mapped reads were quantified at the gene level and summarized to gene counts using STAR-quantMode (GeneCounts), with multimapping and chimeric alignments discarded. The other further analyses were performed in R (v3.6.0). Differential gene expression analysis between WT and cKO NPCs was performed using DESeq2 v1.36.0 with genes whose average counts were lower than the 20 discarded,[61] and identified upregulated and downregulated gene lists between WT and cKO NPCs were used for Gene Ontology (GO) enrichment analysis using Panther v15.0[63,73] (Table S3). Normalized gene counts of genes of selected GO terms calculated by DESeq2 were converted to row Z-scores per gene for visualization in heatmaps. A protein-protein interaction (PPI) network of downregulated genes and pathway enrichment analysis of identified Molecular Complex Detection (MCODE) components of PPI network was performed with Metascape Database.[62]

Mitochondria and cytosolic protein translation assay

Mitochondria protein translation assay was performed as previously described.[32] WT and cKO NPCs cultured on Matrigel-coated plates were incubated in NPC (-Met) medium containing methionine-free DMEM supplemented with 2% B27 supplement, 1% N2 supplement, bFGF (20 ng/mL), EGF (20 ng/mL), 1% GlutaMAX, 1% P/S for 1.5 hours, and then treated with 50 μg/mL cycloheximide, which specifically inhibits cytosolic translation, for 0.5 hour. Then medium was replaced with NPC (-Met) medium containing 50 μg/mL cycloheximide and 500 μM (for Western blot) or 300 μM (for immunostaining) AHA reagent (L-Azidohomoalanine, EMSCO/Fisher, C10102). After 3 hours, cells were washed with PBS for two times and then lysed with cell lysis buffer or fixed with 4% PFA. For Western blotting analysis, after measuring the protein concentration, WT and cKO cell lysates containing the same amount of proteins were reconstituted to the same volume and treated with 50 μM DBCO-PEG4-biotin (Sigma Aldrich Inc) at 37°C for 30 mins. Then 1x sample buffer was added and the protein sample was boiled at 95°C for 10 min and subjected to Western blot analysis. The PVDF membrane was blotted with streptavidin-conjugated HRP at room temperature for 1.5 hours and AHA was visualized by addition of ECL Western blotting Substrate. For staining, the fixed cells were permeabilized with the blocking buffer at room temperature for 1 hour, and then incubated in PBS containing 50 μM DBCO-PEG4-biotin at room temperature for 30 mins. After washing with PBS, the cells were incubated in conjugated-Cy5 streptavidin dissolved in blocking buffer, and then subjected to confocal imaging. Cytosolic protein translation assay was performed similarly, except that 10 μg/mL CAP was used to inhibit the mitochondria protein translation.

Analysis of mitochondria membrane potential

To measure the mitochondria membrane potential (MMP), WT and cKO NPCs with/without piracetam treatment were washed with DMEM/F12 twice and incubated with 50 nM MitoTracker™ Orange CMTMRos (ThermoFisher) dissolved in DMEM/F12 for 30 mins.

Please cite this article in press as: Zhang et al., Epitranscriptomic regulation of cortical neurogenesis via Mettl8-dependent mitochondrial tRNA m^3C modification, Cell Stem Cell (2023), https://doi.org/10.1016/j.stem.2023.01.007

After washing with DMEM/F12, the NPCs were incubated with Accutase for 10 mins and dissociated to single cells. Single cells were suspended by cold Hibernate A Low Fluorescence buffer (Brain Bits) containing 0.1% DAPI (BD, 564907) and then subjected to LSR II Flow Cytometer (BD) for flow cytometry analysis. Forward and side scatter gating was used to identify single cells and live cells were indicated by negative DAPI staining. The signal of Mito-tracker Orange of each cell was measured with the 585/42 channel, and quantification was analyzed with FlowJo software.

Oxygen consumption rate assay

Oxygen consumption rate (OCR) was performed following the manufacturer's instructions for the Agilent seahorse XF96 analyzer. Briefly, WT and cKO NPCs (10^5 cells/well) with/without 1mM piracetam treatment were seeded on Matrigel-coated 96-well seahorse XF96 cell culture microplates. On Day 2, cells were equilibrated in XF DMEM medium (pH 7.4, Agilent) containing 10 mM glucose, 1 mM sodium pyruvate and 2 mM glutamine with/without 1mM piracetam in a non-CO_2 incubator at 37°C for 1 hour. Then the sensory cartridge (Agilent, 102601), which was pre-immersed in seahorse XF calibrant overnight at 37°C, was loaded with appropriate amount of oligomycin, FCCP and rotenone/antimycin A (R/A, Agilent), put into the cell culture microplates and loaded on the seahorse XFe96 analyzer. OCR at the baseline and after sequential injections of 1.5 μM oligomycin, 1 μM FCCP and R/A (0.5 μM each) was monitored with 3 cycles for each step. OCR for each well was normalized to total protein amount as measured with Pierce™ Rapid Gold BCA Protein Assay Kit. The levels of basal, ATP-linked, maximal and spare respiration was calculated accordingly.[36]

Generation of *METTL8* knockout human iPSCs

After washing with PBS, human C1-2 iPSCs were digested with TrypLE (Life Technologies) at 37°C for 5 mins and dissociated to single cells. The single cells were seeded on Matrigel-coated plates and cultured in mTeSR plus medium supplemented with 10 μM Y-27632. On Day 2, culture medium was replaced with 2 mL Opti-Medium containing 10 μM Y-27632, and double PX459 plasmids expressing gRNA targeting *METTL8* gene (as KO) or *AAVS1* locus (as WT) were transfected with LipoStem reagent (Thermo). After 4 hours, 2 mL mTeSR plus medium containing 10 μM Y-27632 was added. On Day 3, mTeSR plus medium containing 10 μM Y-27632 and 0.5 μg/mL puromycin (Millipore) was used to select for puromycin resistant cells. On Day 5 or 6, mTeSR plus medium was added until iPSC clones formed. Several WT and KO clones were picked and seeded on new plates for expansion. The genotype was determined by PCR and knockout of 3rd Exon of *METTL8* was confirmed by qPCR. Only clones with the correct genotype and validated knockout of *METTL8* were maintained and used for organoid generation.

Retrovirus preparation and injection into organoids

To prepare engineered self-inactivating GFP-expressing murine onco-retroviruses,[74] when GP2-293 cells cultured on the 15 cm dish reached ~80% confluence, pSUbGW vectors[57] and pVSV-G Vectors from Retro-X Universal Packaging Vector Set (Clontech) were transfected into GP2-293 cells with Lipofectamine 2000. The culture medium was first changed 6 hours later, and then collected once every 24 hours for three times. The retrovirus in the collected medium was concentrated by ultracentrifugation at 29,000 g for 2 hours, with the supernatant discarded and pellet reconstituted with PBS. The titer of virus was measured by counting the number of infected cell clusters in a serial dilution experiment. Retrovirus GFP mixed with FastGreen and 10 μg/mL Polybrene (Santa Cruz) were microinjected into the lumen of D42 organoids to label dividing cells in the ventricular zone using a calibrated glass micropipette.

QUANTIFICATION AND STATISTICAL ANALYSIS

All the images were analyzed with Photoshop (Adobe), ImageJ (NIH) or Imaris 7.6 software (Bitplane) software. The "Spots" function of Imaris software or the "cell counter" plugin of ImageJ software was used to count the number of cells positive for single or multiple markers. Images were cropped and edited using ImageJ and Adobe Illustrator (Adobe) software.

For analysis of mouse brains, the average value of two sequential sections around bregma -0.10 mm or three sequential sections around bregma -1.06 mm for each mouse brain at embryonic stage or at P1 was used for quantification, respectively. The density of markers$^+$ cells was calculated by the number of markers$^+$ cells in the cortex divided by the area of analyzed cortex. For quantification of mouse brains after in utero electroporation, the average value of three sequential sections from similar regions of WT and cKO brains was used. For quantification of human organoids, because one section may contain GFP$^+$ cells originated from different nearby rosettes, all the GFP$^+$ cells within the image of one section were counted. A range of 56–76 sections from 11–13 different organoids from 3 KO iPSC lines and 4 WT iPSC lines were examined and quantified.

For quantification of immunostaining intensity, tissue sections were attached to the same slides or cells were put into the same well to make sure that the samples being compared were processed in parallel with the same primary/secondary antibodies or reagents; and the corresponding images were taken and processed using the same settings. The sum of intensity of each channel measured with "Measure" function of ImageJ software was used for quantification, and the relative intensity in the KO or drug-treated groups was normalized with that in WT or control groups from the same batch. In Figures 1I and 1J, 1K and 1L, S2K and S2L, and S2P and S2Q, around 50, 100, 100 and 100 cells for each sample in these experiments were quantified, respectively.

For quantification analysis of protein bands in Western blot, the images were cropped with ImageJ software, and the image type was switched to 8-bit. After subtracting the background with setting rolling ball radius as 50.0 pixels, the white and black colors of the images were inverted. Then the intensity of each protein band was measured with "Measure" function of ImageJ, and the sum of intensity of each protein after normalization with that of loading control from the same sample was used for quantification. For

Please cite this article in press as: Zhang et al., Epitranscriptomic regulation of cortical neurogenesis via Mettl8-dependent mitochondrial tRNA m^3C modification, Cell Stem Cell (2023), https://doi.org/10.1016/j.stem.2023.01.007

quantification analysis of protein bands in mitochondria protein translation assay, the normalized intensity of one upper band between 50–75 kD, one middle band between 37–50kD and four lower bands between 15–37 kD were quantified.

No statistical methods were used to predetermine the sample size. For analyzing WT and *Mettl8* cKO mice in each experiment, at least 3 mice and up to 7 mice were included for quantification, and the exact number can be found in the Figure legends. For quantification of human organoids labeled with retrovirus, WT and *METTL8* KO organoids with/without piracetam treatment generated from 3 batches were used, and the number of analyzed sections with different rosettes were shown in Figure legends. The quantification of confocal images was performed blinded to experiment conditions. No data were excluded. For the statistical analysis, an estimate of variation within each group of data is evaluated with standard error of the mean (SEM). Unpaired Student's *t*-test and one-way analysis of variance (ANOVA) was used through GraphPad Prism or Excel software to calculate significant differences as indicated: ns: not significant, $P > 0.05$, *$P < 0.05$, **$P < 0.01$, and ***$P < 0.001$.